Nuclear Physics A572 (1994) 417–458
North-Holland

NUCLEAR PHYSICS A

Competing proton and neutron alignments in neutron-deficient Xe-nuclei

S. Törmänen [a], S. Juutinen [a], R. Julin [a], B. Cederwall [b,c,1], A. Johnson [b,c], R. Wyss [b,c], P. Ahonen [a], B. Fant [d], M. Matsuzaki [e], J. Nyberg [f,2], M. Piiparinen [a,f], S. Mitarai [f,g], J. Mukai [f,g], A. Virtanen [a]

[a] *Department of Physics, University of Jyväskylä, P.O. Box 35, FIN-40351 Jyväskylä, Finland*
[b] *Manne Siegbahn Institute of Physics, S-10405 Stockholm, Sweden*
[c] *The Royal Institute of Technology, Physics Department I, S-10044 Stockholm, Sweden*
[d] *Department of Physics, University of Helsinki, FIN-00170 Helsinki, Finland*
[e] *Department of Physics, Fukuoka University of Education, Munakata, Fukuoka 811-41, Japan*
[f] *The Niels Bohr Institute, Tandem Accelerator Laboratory, DK-4000 Roskilde, Denmark*
[g] *Department of Physics, Kyushu University, Fukuoka 812, Japan*

Received 1 September 1993
(Revised 5 November 1993)

Abstract

High-spin structures of the neutron-deficient ^{117,118,120}Xe isotopes have been studied by in-beam γ-ray spectroscopic techniques. The final nuclei have been identified by means of charged-particle detectors. Collective rotational bands based on the neutron $d_{5/2}$, $g_{7/2}$ and $h_{11/2}$ configurations have been identified in ^{117}Xe. In the even ^{118}Xe and ^{120}Xe nuclei several new side bands were observed and the previously known bands were extended. The present level schemes include two positive-parity bands constructed to high spin in ^{118}Xe, whereas in ^{120}Xe three such bands were observed. In order to explain these bands, both proton and neutron $(h_{11/2})^2$ alignments, as well as the shape degree of freedom, have to be invoked. The possible occurrence of a γS-band is addressed and a pronounced structural change for more heavy Xe-isotopes is discussed. All negative-parity side bands are interpreted in terms of proton two-quasiparticle excitations. The experimental data are compared with total routhian surface calculations.

E

NUCLEAR REACTIONS ^{92}Mo(^{32}S,xn2pα)^{117}Xe,^{118}Xe, (^{32}S,4p), E = 145 MeV; ^{106}Pd(^{18}O,4n), E = 75 MeV; measured E_γ, I_γ, DCO ratios, $\gamma\gamma$-coin. ^{117,118,120}Xe deduced levels, J,π, γ-branching, $B(\lambda)$ ratios, experimental routhians, aligned angular momenta. Enriched targets, array of Compton-suppressed Ge-detectors, 4π array of Si charged-particle detectors, neutron detectors. Total routhian surface calculations. γS-band.

[1] Present address: Lawrence Berkeley Laboratory, Nuclear Science Division, Berkeley, CA 94720, USA.
[2] Present address: Department of Radiation Sciences and The Svedberg Laboratory, Uppsala University, S-75121 Uppsala, Sweden.

SSDI 0375-9474(93)E0675-X

1. Introduction

Nuclei in the $A \approx 120$ region are well suited for studying the effects of shape-driving properties of different quasiparticle configurations. In this region the Fermi surface for the protons lies close to the low-Ω $h_{11/2}$ orbitals, whereas for the neutrons it is situated among the medium-Ω $h_{11/2}$ orbitals. Consequently, band crossings due to the alignment of $h_{11/2}$ neutrons as well as protons are expected at low rotational frequencies. However, the protons and neutrons occupying the $h_{11/2}$ orbits closest to the Fermi surface favour different nuclear shapes. The shape evolution of the Xe-isotopes predicted by mean-field calculations [1] is quite in contrast to the smooth parameter dependence obtained by the IBA-model calculations in this mass region [2,3]. However, a recent investigation of odd Xe- and Ba-isotopes also yield a sudden change in the IBA-model parameters [4].

Recently, band crossings in several Cs-, Ba- and La-nuclei in the mass $A \approx 120$ region have been investigated, and proton and neutron crossings were observed to take place around $\hbar\omega = 0.35$ and 0.45 MeV, respectively [5–9]. In the neutron-deficient Xe-isotopes the alignment occurring at the lowest frequency is believed to be due to the $h_{11/2}$ neutrons [10,11], while the role of the $h_{11/2}$ protons in low-lying band crossings has remained unclear. The situation is further complicated by the existence of a low-lying γ-vibrational band, the continuation of which to high spins will be discussed within RPA-model calculations.

Although the ^{117,118,120}Xe isotopes have previously been investigated in heavy-ion induced reactions [10–15], the knowledge of the high-spin properties was quite limited. In the present study the level schemes of these nuclei were largely extended by using the NORDBALL Ge-detector array together with particle detectors. We have found that the neutron-deficient Xe-nuclei show both proton and neutron alignments at about the same rotational frequency. Some of the results have already been reported elsewhere [16,17].

2. Experimental methods

Excited states in ^{117,118,120}Xe were populated by bombarding a 98% enriched, self-supporting 1.2 mg/cm^2 thick ^{92}Mo target with a ^{32}S beam of 145 MeV energy. The ^{32}S beam was provided by the FN tandem plus booster accelerator system at the Niels Bohr Institute, Denmark. The γ-rays were detected in the NORDBALL detector array. In the present experiment the array consisted of 15 Compton-suppressed Ge-detectors mounted at three different rings at 79°, 101° and 143° with respect to the beam direction.

In compound-nucleus reactions leading to very neutron-deficient nuclei charged-particle emission is dominant and many reaction channels are open. For providing unambiguous assignments of γ-rays to certain final nuclei and for cleaning the data from undesired channels, the detection and identification of evaporated particles is crucial. Therefore, for detecting charged particles the NORDBALL detector system was complemented with a Si-detector ball [18] consisting of 17 elements placed inside the Ge-detector system. The average distance from the target to the Si-detectors was 2 cm. Each Si-detector, having

a 170 μm depletion thickness, was covered with a thin Au-foil preventing the scattered heavy ions from reaching the Si-detectors. The experimental setup included also a neutron detector system [19] consisting of 11 liquid scintillator detectors. The neutron multiplicity information was not used for the Xe-nuclei, however, this information was crucial for identification of some other nuclei from this experiment [6,7,20].

The recoiling nuclei were stopped in an Au-stopper 4 cm down stream from the centre of the detector system. In the geometry used here the Ge-detectors in the ring at 143° had a full view of the stopper, while the detectors at the other angles could see the stopper only partly or not at all. This provides a chance to observe isomeric decays within the coincidence time window of about 100 ns.

An event was written on the magnetic tape whenever at least two γ-rays were detected in coincidence with a charged particle. About 125 million events were collected in the experiment. In the off-line analysis, coincidence matrices were sorted using different particle conditions. In some matrices the statistics was relatively poor which, however, was greatly compensated by the cleanness of the data.

Excited states in ^{120}Xe were also populated by using the ^{106}Pd(^{18}O,4n)^{120}Xe reaction at a beam energy of 75 MeV. The target was a 97% enriched self-supporting ^{106}Pd foil with a thickness of 1.1 mg/cm^2. In this experiment 20 Compton-suppressed Ge-detectors were mounted in the NORDBALL frame at four different angles. The total γ-ray energy and multiplicity were measured for each $\gamma\gamma$-coincidence event by an inner BaF_2 ball consisting of 53 elements. This provided partial separation between the 4n-channel leading to ^{120}Xe and disturbing 3n-, p2n- and p3n-channels populating states in ^{121}Xe, ^{121}I and ^{120}I, respectively. In this experiment about 150 million events were collected.

The transition multipolarities were inferred from the measured DCO ratios. For deducing the DCO ratios the data were sorted into two matrices. The first matrix contained the coincident γ-ray pairs, where one of the γ-rays was detected at 143° (x-parameter), and the second matrix contained events, where one of the γ-rays had hit a detector mounted at 79° or 101° (x-parameter). In both matrices the y-parameter was the other γ-ray in the coincidence event. In this way all the data collected in the experiment could be used for deducing the DCO ratios. Coincidence spectra were then constructed by setting identical y-gates in both matrices. In each rotational band several gates were set on clean transitions. For the weakest transitions gated spectra were also summed to gain better statistics. The DCO ratio is defined as

$$R(E_\gamma) = \frac{I_\gamma(E_\gamma; 143°)}{I_\gamma(E_\gamma; \approx 90°)}. \tag{1}$$

The DCO ratio was normalized to $R = 1.0$ for stretched E2 transitions at high spin. Within this normalization a value of $R \approx 0.6$ is expected for the stretched dipole transitions.

3. The level schemes

3.1. THE NUCLEUS ^{117}Xe

The level scheme of ^{117}Xe shown in Fig. 1 was constructed from the α2p and αp gated $\gamma\gamma$-coincidence matrices. In these matrices transitions belonging to ^{118}Xe are dominating. The strongest transitions in ^{117}Xe have intensities of about 10% of the $2^+ \rightarrow 0^+$ transition in ^{118}Xe. Examples of background-subtracted spectra are presented in Fig. 2 and the γ-rays assigned to ^{117}Xe are listed in Table 1.

The ground state of ^{117}Xe has been assigned to have spin and parity $\frac{5}{2}^{(+)}$ [21]. The decay from the $\frac{11}{2}^-$ state of band 1 into the ground state clearly indicates that the ground state cannot belong to band 1. Since band 1 is the only negative-parity band expected near the yrast line, the positive-parity assignment for the ground state is favoured. This is further supported by comparison to neighbouring nuclei. The magnetic moment of $-0.594\ \mu_N$ indicates predominantly a $d_{5/2}$ ($\frac{5}{2}^+[402]$) character, with some admixture of the $g_{7/2}$ ($\frac{5}{2}^+[413]$) orbital. In the present experiment two low-lying positive-parity structures (bands 3, 4) were observed. Some of the lowest states in these bands have previously been observed in β-decay work [13].

The yrast band (band 1) is based on the $\frac{5}{2}^-[532]$ or $\frac{3}{2}^-[541]$ configuration emanating

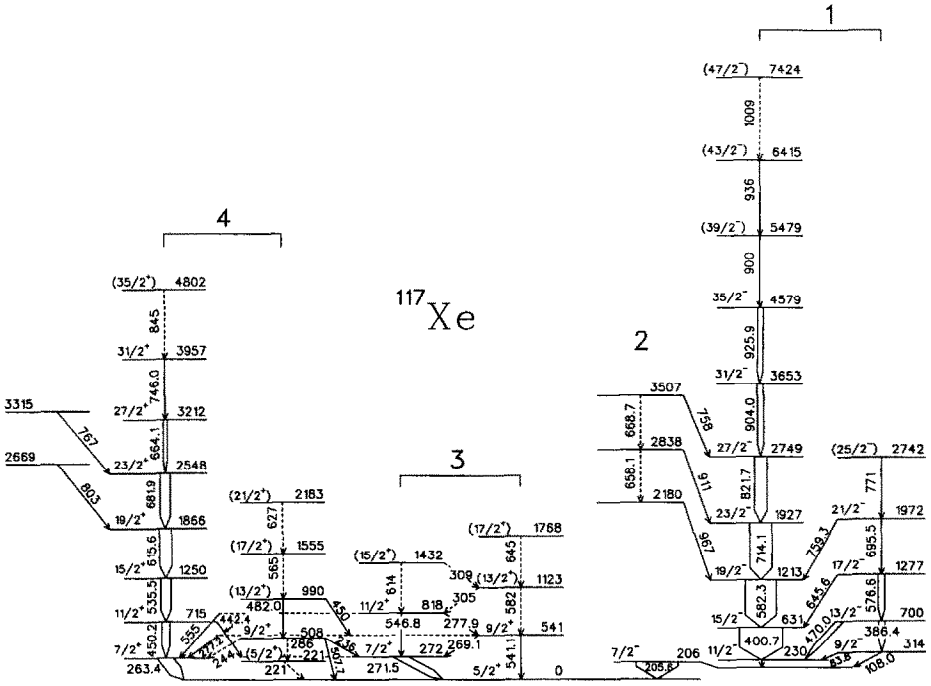

Fig. 1. The level scheme of ^{117}Xe. Energies are in keV.

TABLE 1

The γ-ray energies, intensities and DCO ratios for the transitions assigned to ^{117}Xe. The intensities are obtained from the axis spectrum for the strongest transitions and for the other transitions from the coincidence spectra

E_γ	I_γ	DCO ratio	Assigned $I_i \rightarrow I_f$	Band
83.8	3.9(3)		$\frac{9}{2}^- \rightarrow \frac{11}{2}^-$	1
108.0	1.3(2)		$\frac{9}{2}^- \rightarrow \frac{7}{2}^-$	1
205.6	97.8(10)		$\frac{7}{2}^- \rightarrow \frac{5}{2}^+$	1→3
221			$(\frac{5}{2}^+) \rightarrow \frac{5}{2}^+$	4→3
236	1.8(3)	0.34(8)	$\frac{9}{2}^+ \rightarrow \frac{7}{2}^+$	4→3
244	< 1		$\frac{9}{2}^+ \rightarrow \frac{7}{2}^+$	4
263.4	29.0(3)	0.52(4)	$\frac{7}{2}^+ \rightarrow \frac{5}{2}^+$	4→3
269.1	2.7(3)	0.45(6)	$\frac{9}{2}^+ \rightarrow \frac{7}{2}^+$	3
271.5	18.4(5)	0.46(7)	$\frac{7}{2}^+ \rightarrow \frac{5}{2}^+$	3
277.2	2.1(4)	0.32(9)	$\frac{9}{2}^+ \rightarrow \frac{7}{2}^+$	3→4
277.9			$\frac{11}{2}^+ \rightarrow \frac{9}{2}^+$	3
286			$\frac{9}{2}^+ \rightarrow (\frac{5}{2}^+)$	4
305			$(\frac{13}{2}^+) \rightarrow \frac{11}{2}^+$	3
309			$(\frac{15}{2}^+) \rightarrow (\frac{13}{2}^+)$	3
386.4	14.5(7)	1.06(11)	$\frac{13}{2}^- \rightarrow \frac{9}{2}^-$	1
400.7	100	0.84(4)	$\frac{15}{2}^- \rightarrow \frac{11}{2}^-$	1
442.4	8.7(6)	0.83(7)	$\frac{11}{2}^+ \rightarrow \frac{7}{2}^+$	4→3
450			$(\frac{13}{2}^+) \rightarrow \frac{9}{2}^+$	4→3
450.2	18.6(6)	0.86(5)	$\frac{11}{2}^+ \rightarrow \frac{7}{2}^+$	4
470.0	14.4(14)	0.48(7)	$\frac{13}{2}^- \rightarrow \frac{11}{2}^-$	1
482.0	5.0(10)	1.1(3)	$(\frac{13}{2}^+) \rightarrow \frac{9}{2}^+$	4
507.7	4.5(5)		$\frac{9}{2}^+ \rightarrow \frac{5}{2}^+$	4→3
535.5	24.6(8)	0.92(6)	$\frac{15}{2}^+ \rightarrow \frac{11}{2}^+$	4
541.1			$\frac{9}{2}^+ \rightarrow \frac{5}{2}^+$	3
546.8	3.9(3)	1.24(14)	$\frac{11}{2}^+ \rightarrow \frac{7}{2}^+$	3
555	1.8(4)		$\frac{11}{2}^+ \rightarrow \frac{7}{2}^+$	3→4
565	4.8(3)		$(\frac{17}{2}^+) \rightarrow (\frac{13}{2}^+)$	4
576.6	16.0(20)	0.94(14)	$\frac{17}{2}^- \rightarrow \frac{13}{2}^-$	1
582			$(\frac{13}{2}^+) \rightarrow \frac{9}{2}^+$	3
582.3	72.0(12)	0.96(4)	$\frac{19}{2}^- \rightarrow \frac{15}{2}^-$	1

TABLE 1—continued

E_γ	I_γ	DCO ratio	Assigned $I_i \rightarrow I_f$	Band
614	2.4(5)		$(\frac{15}{2}^+) \rightarrow \frac{11}{2}^+$	3
615.6	28.8(6)	0.99(7)	$\frac{19}{2}^+ \rightarrow \frac{15}{2}^+$	4
627	3.6(6)		$(\frac{21}{2}^+) \rightarrow (\frac{17}{2}^+)$	4
645			$(\frac{17}{2}^+) \rightarrow (\frac{13}{2}^+)$	3
645.6	7.1(4)	0.25(10)	$\frac{17}{2}^- \rightarrow \frac{15}{2}^-$	1
658.1	5.6(4)	1.10(14)		2
664.1	9.6(12)	1.13(14)	$\frac{27}{2}^+ \rightarrow \frac{23}{2}^+$	4
668.7	5.4(4)	1.10(15)		2
681.9	24.3(6)	0.92(8)	$\frac{23}{2}^+ \rightarrow \frac{19}{2}^+$	4
695.5	6.7(5)	1.23(20)	$\frac{21}{2}^- \rightarrow \frac{17}{2}^-$	1
714.1	51.8(10)	0.95(4)	$\frac{23}{2}^- \rightarrow \frac{19}{2}^-$	1
746.0	3.0(6)	1.00(15)	$\frac{31}{2}^+ \rightarrow \frac{27}{2}^+$	4
758	3.1(9)		$\rightarrow \frac{27}{2}^-$	$2 \rightarrow 1$
759.3	8.1(14)	0.97(10)	$\frac{21}{2}^- \rightarrow \frac{19}{2}^-$	1
767	5.4(6)	0.9(2)	$\rightarrow \frac{23}{2}^+$	$\rightarrow 4$
771	2(1)		$(\frac{25}{2}^-) \rightarrow \frac{21}{2}^-$	1
803	3.3(7)		$\rightarrow \frac{19}{2}^+$	$\rightarrow 4$
821.7	29.0(7)	1.03(5)	$\frac{27}{2}^- \rightarrow \frac{23}{2}^-$	1
845	2.7(7)		$(\frac{35}{2}^+) \rightarrow \frac{31}{2}^+$	4
900	5.0(15)		$(\frac{39}{2}^-) \rightarrow \frac{35}{2}^-$	1
904.0	15.1(14)	1.00(5)	$\frac{31}{2}^- \rightarrow \frac{27}{2}^-$	1
911	2.9(6)		$\rightarrow \frac{23}{2}^-$	$2 \rightarrow 1$
925.9	12.9(7)	0.87(11)	$\frac{35}{2}^- \rightarrow \frac{31}{2}^-$	1
936	0.8(4)		$(\frac{43}{2}^-) \rightarrow (\frac{39}{2}^-)$	1
967	4.4(5)		$\rightarrow \frac{19}{2}^-$	$2 \rightarrow 1$
1009	1.0(5)		$(\frac{47}{2}^-) \rightarrow (\frac{43}{2}^-)$	1

from the neutron $h_{11/2}$ state. This band was tentatively observed up to the $\frac{47}{2}^-$ and $\frac{25}{2}^-$ states in the favoured ($\alpha = -\frac{1}{2}$) and unfavoured ($\alpha = \frac{1}{2}$) signatures, respectively. In an earlier experiment by Chowdhury et al. [12] this band has been identified up to the $\frac{27}{2}^-$ and $\frac{21}{2}^-$ states in the favoured and unfavoured signature, respectively. The bottom part of the band has so far remained unclear. The shape of the 205.6 keV line in the Doppler corrected spectrum of Fig. 2a indicates the existence of an isomer. Chowdhury

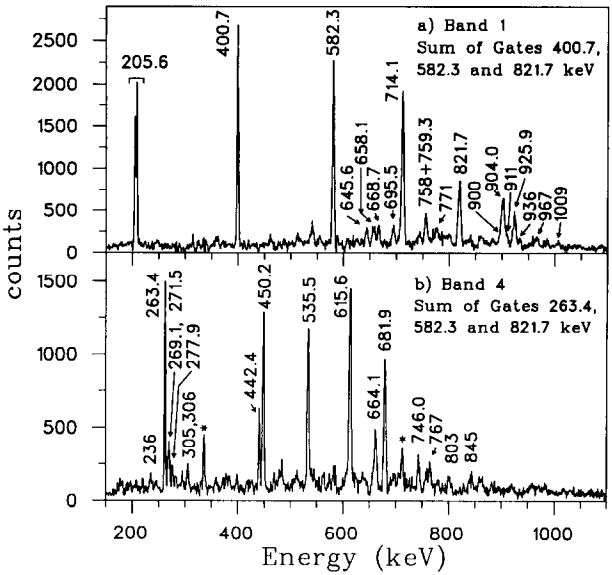

Fig. 2. Sample coincidence spectra for ^{117}Xe. The peaks labelled by energy are placed in the ^{117}Xe level scheme. The peaks labelled with an asterisk are due to contaminants.

et al. [12] proposed that the state at 205.6 keV would be the $\frac{11}{2}^-$ member of the $h_{11/2}$ band. However, in the β-decay work by Marquier et al. [13] the 206 keV state was assigned to have $I^\pi = \frac{7}{2}^-$. In our experiment a weak 108.0 keV transition (c.f. also ref. [13]) was observed in coincidence with the 205.6 and 386.4 keV transitions. We propose that this 108.0 keV line is due to the $\frac{9}{2}^- \rightarrow \frac{7}{2}^-$ transition. Consequently, the decay from the $\frac{11}{2}^-$ state to the $\frac{7}{2}^-$ state proceeds via an unobserved 24 keV E2 transition. The 108.0 keV transition passes the isomeric state, since in the spectrum gated on this transition, the 205.6 keV line has only the flight component. Thus it is the state at 230 keV which has the isomeric character. From the intensity of the 205.6 keV transition in different spectra we estimate that the half-life of the isomeric state is less than 100 ns. Comparing to ^{119}Xe [22] and assuming a similar reduced transition rate for the $\frac{11}{2}^- \rightarrow \frac{7}{2}^-$ transition a lifetime of about 80 ns is expected for the $\frac{11}{2}^-$ state in ^{117}Xe.

Band 2 shows only two transitions. This band is connected to band 1 by three transitions, whose character could not be determined.

3.2. THE NUCLEUS ^{118}Xe

Information on the nucleus ^{118}Xe was obtained from the αp- and α2p-gated coincidence matrices. The level scheme of ^{118}Xe is shown in Fig. 4. The γ-rays assigned to ^{118}Xe are listed in Table 2 together with their DCO ratios. Examples of background-subtracted spectra are presented in Fig. 3.

TABLE 2

The γ-ray energies, intensities and DCO ratios for the transitions assigned to ^{118}Xe. The intensities are obtained from the axis spectrum for the strongest transitions and for the other transitions from the spectra gated on the lowest transitions in each band

E_γ	I_γ	DCO ratio	Assigned $I_i \rightarrow I_f$	Band
150.8	<1.2		$\rightarrow 5^-$	$\rightarrow 2$
157.3	<1		$9^- \rightarrow (8^-)$	1
190.7	<1		$10^- \rightarrow$	$1 \rightarrow$
246.7	3.2(2)	0.67(3)	$10^- \rightarrow 9^-$	1
255.5	1.1(2)	1.0(2)	$12^+ \rightarrow 12^+$	$4 \rightarrow$ Y
268.8	4.1(2)	0.61(3)	$11^- \rightarrow 10^-$	1
287.0	3.8(3)	0.71(8)	$9^- \rightarrow 9^-$	$1 \rightarrow 2$
319.5	3.7(2)	0.70(3)	$12^- \rightarrow 11^-$	1
337.6	105(2)	0.68(1)	$2^+ \rightarrow 0^+$	Y
344.7	3.5(2)	0.63(4)	$13^- \rightarrow 12^-$	1
384.6	3.0(2)	0.62(4)	$14^- \rightarrow 13^-$	1
403.9	2.3(3)		$10^- \rightarrow (8^-)$	1
407.1	2.2(2)	0.83(7)	$15^- \rightarrow 14^-$	1
418.5	1.6(5)		$(8^-) \rightarrow$	$1 \rightarrow$
423.9	1.4(2)	1.0(2)	$7^- \rightarrow 5^-$	2
438.5	2.5(3)	0.80(15)	$10^+ \rightarrow 10^+$	$4 \rightarrow$ Y
439	<1		$3^+ \rightarrow 2^+$	γ
441.7	1.4(3)	0.53(4)	$16^- \rightarrow 15^-$	1
457.3	1.2(3)	1.2(4)	$(8^-) \rightarrow (6^-)$	3
457.7	1.3(2)	0.96(15)	$17^- \rightarrow 16^-$	1
473.1	100(2)	0.83(1)	$4^+ \rightarrow 2^+$	Y
487.9	<1			
488	1.2(2)	1.0(2)	$18^- \rightarrow 17^-$	1
490	1.2(2)	1.0(2)	$19^- \rightarrow 18^-$	1
501.0	11.5(4)	0.83(3)	$9^- \rightarrow 7^-$	2
513.3	1.9(4)		$4^+ \rightarrow 2^+$	γ
515.4	4.7(5)	1.11(15)	$11^- \rightarrow 9^-$	1
539.2	3.5(5)	1.05(12)	$(10^-) \rightarrow (8^-)$	3
547	<1		$(6^-) \rightarrow 5^-$	$3 \rightarrow 2$
556.5	5.5(10)		$6^+ \rightarrow 4^+$	γ
557.2	2.0(5)		$5^+ \rightarrow 3^+$	γ
558	<1		$3^+ \rightarrow 4^+$	$\gamma \rightarrow$ Y
587.0	94.8(8)	0.92(1)	$6^+ \rightarrow 4^+$	Y
588	4.5(8)	0.91(2)	$12^- \rightarrow 10^-$	1
591.5	2.4(4)		$2^+ \rightarrow 2^+$	$\gamma \rightarrow$ Y

TABLE 2—continued

E_γ	I_γ	DCO ratio	Assigned $I_i \rightarrow I_f$	Band
593.0	7.0(4)	0.85(4)	$12^+ \rightarrow 10^+$	4
600.8	1.9(3)	0.53(7)	$6^+ \rightarrow 6^+$	$\gamma \rightarrow$Y
623.2	20.1(8)	0.84(2)	$11^- \rightarrow 9^-$	2
628.0	5.5(1)		$8^+ \rightarrow 6^+$	γ
629.5	4.5(1)		$10^+ \rightarrow 8^+$	$4 \rightarrow \gamma$
631.7	4.0(1)		$4^+ \rightarrow 4^+$	$\gamma \rightarrow$ Y
637.6	5.8(4)	0.99(6)	$(12^-) \rightarrow (10^-)$	3
638.2	2.8(3)		$7^+ \rightarrow 5^+$	γ
664.6	5.3(8)	0.92(10)	$13^- \rightarrow 11^-$	1
676.9	67.9(12)	0.96(1)	$8^+ \rightarrow 6^+$	Y
682	1.6(5)		$9^+ \rightarrow 7^+$	γ
692.3	7.2(5)	0.91(4)	$14^+ \rightarrow 12^+$	4
710	<1		$(11^+) \rightarrow (9^+)$	γ
719.2	18.7(9)	0.97(3)	$13^- \rightarrow 11^-$	2
727	<1		$11^- \rightarrow 10^+$	2→Y
730	6.4(12)	0.94(6)	$14^- \rightarrow 12^-$	1
736.9	5.7(5)		$(14^-) \rightarrow (12^-)$	3
742.8	40.9(8)	0.95(2)	$10^+ \rightarrow 8^+$	Y
776.2	27.4(8)	1.01(2)	$12^+ \rightarrow 10^+$	Y
776.2	24.1(8)	1.01(2)	$14^+ \rightarrow 12^+$	Y
780	<1		$21^- \rightarrow$	2→
788.1	16.7(10)	1.01(2)	$16^+ \rightarrow 14^+$	Y
791.8	4.1(7)	1.04(15)	$15^- \rightarrow 13^-$	1
796.7	11.2(5)	1.08(4)	$15^- \rightarrow 13^-$	2
815.8	6.6(6)	0.94(8)	$16^+ \rightarrow 14^+$	4
826.8	3.9(4)		$(16^-) \rightarrow (14^-)$	3
843	2.4(4)		$(18^-) \rightarrow (16^-)$	3
846.4	20(2)	0.59(6)	$9^- \rightarrow 8^+$	2→Y
847.2	11(2)	1.01(5)	$18^+ \rightarrow 16^+$	Y
849	2.7(8)	0.73(3)	$16^- \rightarrow 14^-$	1
860.6	3.7(3)	0.94(8)	$21^- \rightarrow 19^-$	2
862	2.6(4)		$(20^-) \rightarrow (18^-)$	3
867.8	7.4(4)	1.03(5)	$17^- \rightarrow 15^-$	2
886.7	4.8(3)	0.85(4)	$19^- \rightarrow 17^-$	2
899.3	3.5(8)	0.89(6)	$17^- \rightarrow 15^-$	1
909	1.5(3)		$(22^-) \rightarrow (20^-)$	3
925.8	6.9(8)		$(8^-) \rightarrow 8^+$	3→Y
929	<1		$2^+ \rightarrow 0^+$	$\gamma \rightarrow$ Y

TABLE 2—continued

E_γ	I_γ	DCO ratio	Assigned $I_i \rightarrow I_f$	Band
929.6	4.2(6)	1.06(5)	$18^+ \rightarrow 16^+$	4
931.8	6.3(7)	1.02(4)	$20^+ \rightarrow 18^+$	Y
946	2.9(9)	0.99(10)	$18^- \rightarrow 16^-$	1
967.2	1.6(3)		$\rightarrow 17^-$	$\rightarrow 2$
978	2.0(7)	1.1(2)	$19^- \rightarrow 17^-$	1
989.9	2.5(3)	0.97(7)	$23^- \rightarrow 21^-$	2
1020	<1		$(24^-) \rightarrow (22^-)$	3
1022.3	16.0(10)	0.56(5)	$7^- \rightarrow 6^+$	$2 \rightarrow$ Y
1023.5	7.0(10)	1.01(7)	$22^+ \rightarrow 20^+$	Y
1031	<1		$3^+ \rightarrow 2^+$	$\gamma \rightarrow$ Y
1032.7	2.1(3)	0.85(8)	$20^+ \rightarrow 18^+$	4
1094	<1		$(22^+) \rightarrow 20^+$	4
1104.9	<1		$4^+ \rightarrow 2^+$	$\gamma \rightarrow$ Y
1113.1	2.0(4)		$5^+ \rightarrow 4^+$	$\gamma \rightarrow$ Y
1115.3	4.3(2)	1.02(6)	$24^+ \rightarrow 22^+$	Y
1118	2.4(4)	1.04(15)	$25^- \rightarrow 23^-$	2
1133.6	3.3(4)	0.48(9)	$9^- \rightarrow 8^+$	$1 \rightarrow$ Y
1145	<1		$(6^-) \rightarrow 6^+$	$3 \rightarrow$ Y
1156	1.8(3)	1.2(2)	$27^- \rightarrow 25^-$	2
1185.4	2.7(5)	0.6(2)	$5^- \rightarrow 4^+$	$2 \rightarrow$ Y
1188	2.0(5)		$\rightarrow 8^+$	$\rightarrow$ Y
1196	<1.2		$(29^-) \rightarrow 27^-$	2
1199.0	3.2(2)	1.01(9)	$26^+ \rightarrow 24^+$	Y
1235	2.0(5)		$\rightarrow 6^+$	$\rightarrow$ Y
1262.3	2.1(2)	0.86(13)	$30^+ \rightarrow 28^+$	Y
1272.7	1.9(2)		$(32^+) \rightarrow 30^+$	Y
1281	<1		$(31^-) \rightarrow (29^-)$	2
1284.4	2.7(2)	0.8(2)	$28^+ \rightarrow 26^+$	Y
1312	<1.1		$(34^+) \rightarrow (32^+)$	Y

The yrast band of ^{118}Xe could be extended from the known 16^+ state [10] up to the tentative $I^\pi = (34^+)$ state when assuming a continuation of stretched E2 transitions above $I^\pi = 30^+$. At lower spins the E2 character of the yrast band transitions is evident from the DCO ratios.

The negative-parity band 2 could be extended from the known 5928 keV state by 7 new transitions up to the state at 13416 keV in excitation energy. The observed DCO ratios for the transitions from the states at 2420 and 2921 keV to the ground-state band

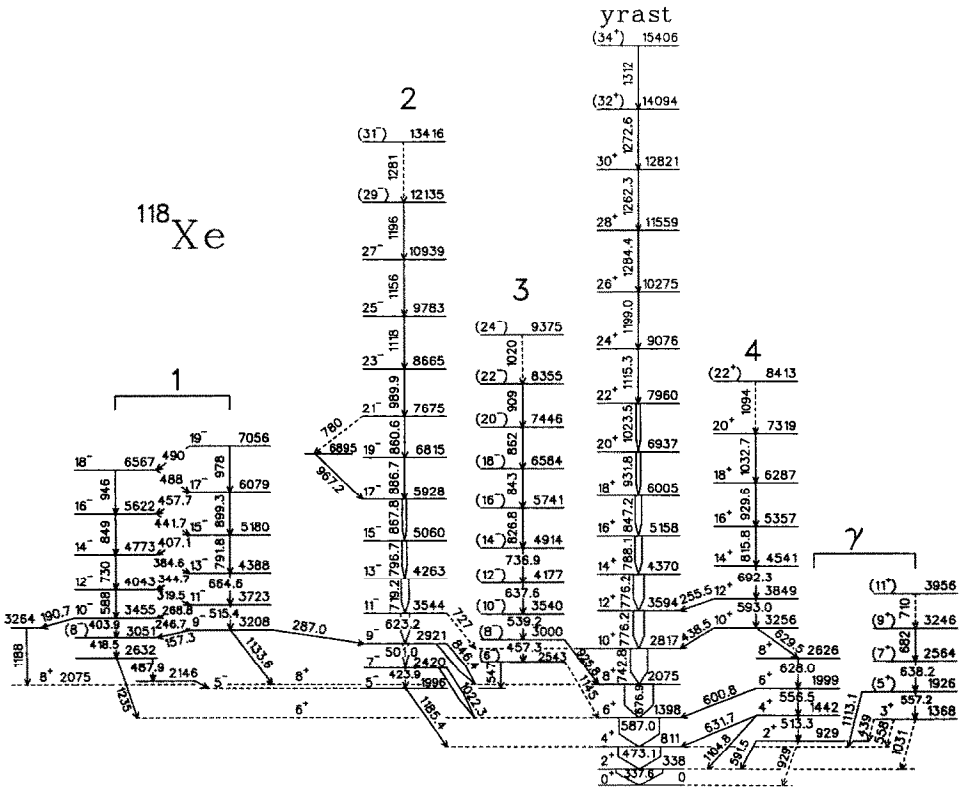

Fig. 3. The level scheme of ^{118}Xe. Energies are in keV.

(g.s. band) support the previous spin and parity assignment of ref. [10].

The weakly populated band 3 has most likely negative parity and might be the signature partner of band 2. Note, that a very similar band is observed in ^{120}Xe (see subsect. 3.3). The properties of the negative-parity bands are discussed more in details below.

Band 1, which consists of two $\Delta I = 2$ cascades connected by $\Delta I = 1$ transitions, was previously known from the 3208 keV level up to the 4388 keV level [10]. This band was extended with seven new high spin states. At the bottom of the band one new state at 3051 keV was added. The spin assignments in this band are based on the DCO ratio of the 1133.6 and 287.0 keV transitions. A part of the intensity of band 1 is not accounted for by the observed transitions decaying out of this band. This implies, that there must be more levels below band 1, which are not identified in our experiment.

In the present work the previous results of ref. [10] for the γ-band were confirmed.

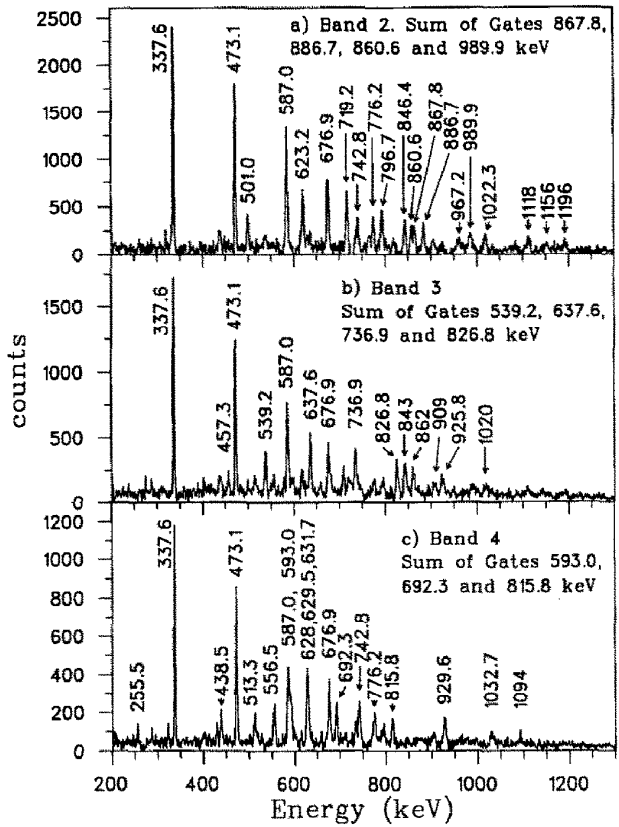

Fig. 4. Sample coincidence spectra for ^{118}Xe. The peaks labelled by energy are placed in the ^{118}Xe level scheme.

Furthermore, the $\alpha = 1$ sequence was extended by one transition.

Band 4 was earlier known up to the 5357 keV level and it was tentatively assigned to have even spins and positive parity [10]. In the present study this band was extended by three transitions. Our data support the earlier spin and parity assignment, since the DCO ratio of the 628.0+629.5 keV transitions is close to unity as expected for stretched E2 transitions. The DCO ratios for the 438.5 and 255.5 keV transitions are also consistent with the adopted spin values. It should be noted that no transition from the 10^+ state of band 4 to the 8^+ state of the yrast band was observed.

3.3. THE NUCLEUS ^{120}Xe

The level scheme of ^{120}Xe, as obtained in the present investigation using the ^{92}Mo(^{32}S,4p) and ^{106}Pd(^{18}O,4n) reactions, is displayed in Fig. 5. In the former reaction a very clean

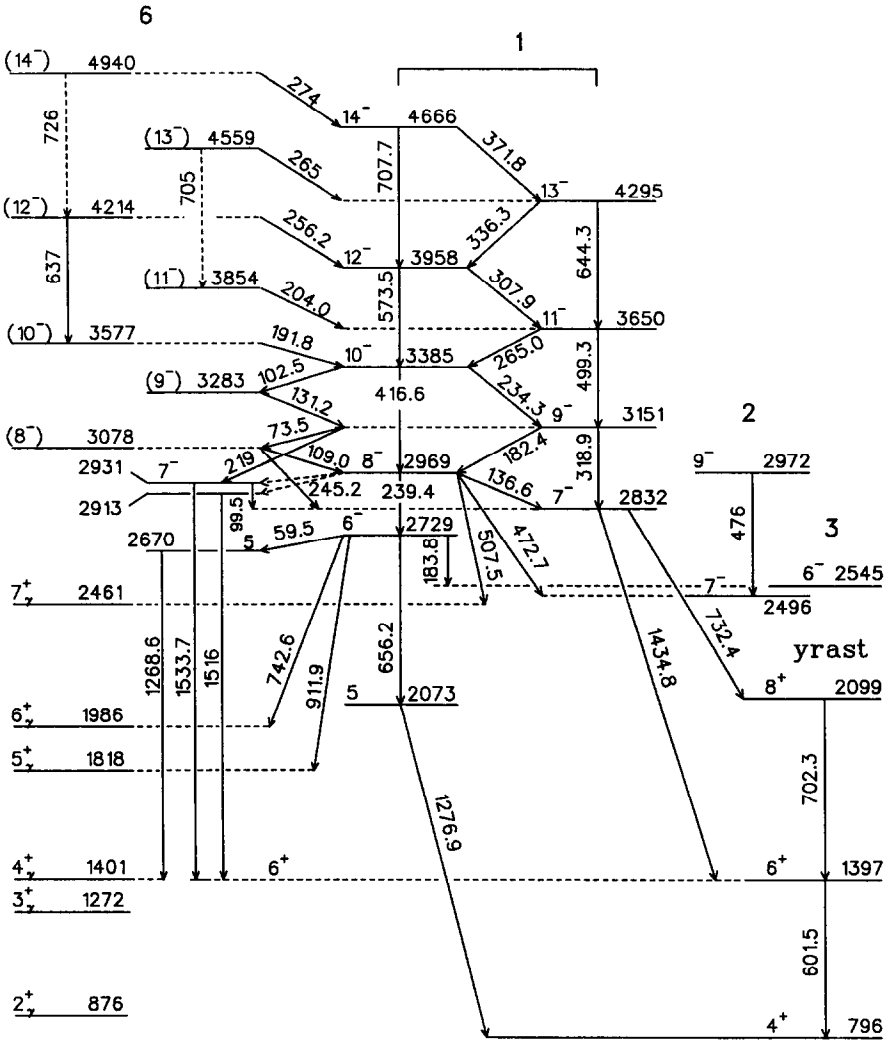

Fig. 5. The level scheme of ^{120}Xe obtained in the present work.

coincidence matrix, with rather poor statistics, was obtained for ^{120}Xe by requiring four protons in coincidence with γ-rays. The latter measurement gave much better statistics. A number of new transitions could be added to the previous level scheme [11,14,15] of ^{120}Xe. Our level scheme departs in many details from that of Goswamy et al. recently published as a short note [15]. The γ-rays assigned to ^{120}Xe in the present study are listed in Table 3 together with their DCO ratios. A sample of coincidence spectra is shown in Figs. 6 and 7. In Figs. 5 and 3 the related bands have the same labelling. Additional bands in ^{120}Xe are labelled as 5 and 6.

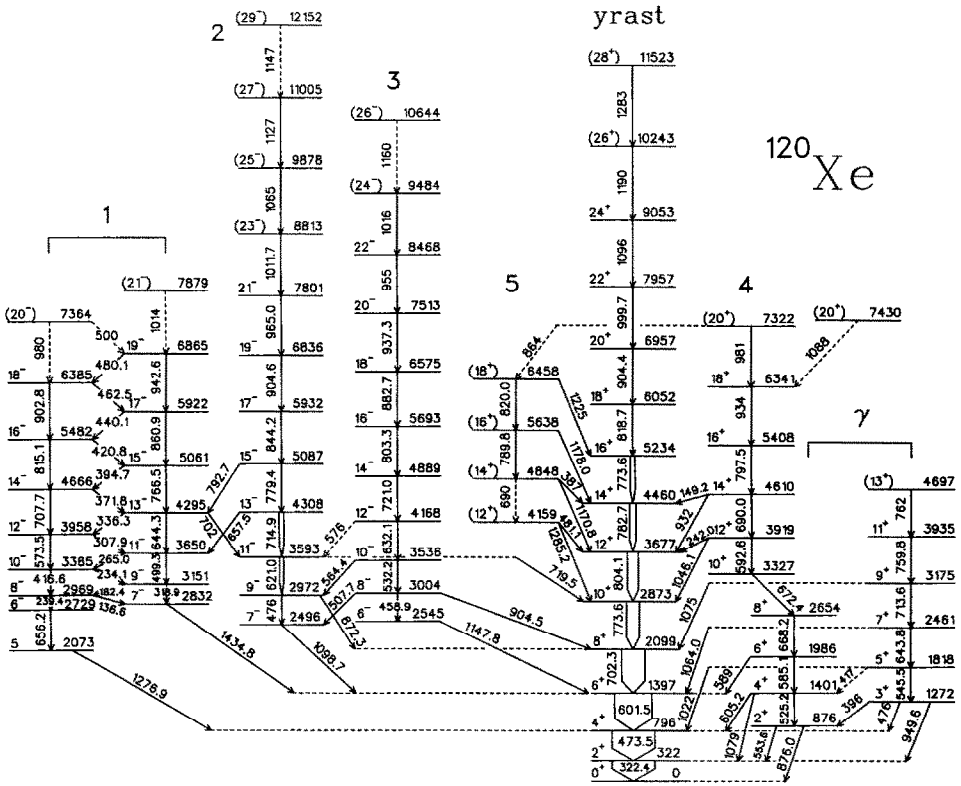

Fig. 5 — continued.

supported. We have observed the 1096 and 1190 keV transitions and a new 1283 keV transition to be in cascade above the $I^{\pi} = 22^{+}$ state.

The second positive-parity band (band 4) decays at $I = 12$ and $I = 14$ to the yrast band and at spin 10 to the γ-band, which is in disagreement with the scheme of Goswamy et al. [15]. They suggest that a sequence of the 798.1 and 933.0 keV transitions would feed the yrast 12^{+} state via a 689.5 keV transition, whereas we observed transitions of about the same energies in coincidence with the even-spin sequence of the γ-band, see Fig. 6. The 242.0 and 1046.1 keV transitions present in the summed spectrum gated on the 592.6 and 690.3 keV transitions emanate from the latter gate. Note, that the 592.6 and 672.4 keV transitions were previously placed in the γ-band [14,15]. The DCO ratios

The yrast band in ^{120}Xe was extended to $I^{\pi} = (28^{+})$. A spectrum gated on the $22^{+} \rightarrow 20^{+}$ transition is shown in Fig. 6. Our level scheme for this band up to $I = 22^{+}$ is in agreement with that of Goswamy et al. [15]. Above $I^{\pi} = 22^{+}$ they have placed the 1095 and 1190.8 keV transitions in parallel and a 1097 keV transition in cascade with the latter one. In the present work, the existence of the 1095+1097 keV doublet was not

TABLE 3

The γ-ray energies, intensities and DCO ratios for the transitions assigned to ^{120}Xe from the ^{106}Pd(^{18}O,4n) reaction. The intensities are obtained from the axis spectrum for the strongest transitions and for the other transitions from the coincidence spectra

E_γ	I_γ	DCO ratio	Assigned $I_i \rightarrow I_f$	Band
59.5	0.3(1)		$6^- \rightarrow 5$	1→6
73.5	1.3(3)		$9^- \rightarrow (8^-)$	1→6
99.5	0.4(1)	1.0(2)	$7^- \rightarrow 7^-$	6→1
102.5	0.6(2)	0.48(8)	$10^- \rightarrow (9^-)$	1→6
109.0	1.8(1)	1.21(12)	$(8^-) \rightarrow 8^-$	6→1
131.2	0.8(2)	1.2(2)	$(9^-) \rightarrow 9^-$	6→1
136.6	1.8(1)	0.52(4)	$8^- \rightarrow 7^-$	1
149.2	0.7(2)	1.22(8)	$14^+ \rightarrow 14^+$	4→Y
182.4	6.1(2)	0.93(6)	$9^- \rightarrow 8^-$	1
183.8	0.3(1)	0.82(11)	$6^- \rightarrow 6^-$	1→3
191.8	0.7(1)	1.00(9)	$(10^-) \rightarrow 10^-$	6→1
204.0	0.7(1)	0.94(12)	$(11^-) \rightarrow 11^-$	6→1
219	0.2(1)		$9^- \rightarrow 7^-$	1→6
234.1	9.0(3)	0.76(3)	$10^- \rightarrow 9^-$	1
239.4	3.5(5)	0.85(5)	$8^- \rightarrow 6^-$	1
242.0	1.0(2)	1.05(19)	$12^+ \rightarrow 12^+$	4→Y
245.2	0.4(1)		$(8^-) \rightarrow 7^-$	6→1
256.2	0.5(1)	0.76(10)	$(12^-) \rightarrow 12^-$	6→1
265.0	6.9(3)	0.74(3)	$11^- \rightarrow 10^-$	1
265	0.7(2)		$(13^-) \rightarrow 13^-$	6→1
274	<0.5		$\rightarrow 14^-$	6→1
307.9	6.1(3)	0.66(3)	$12^- \rightarrow 11^-$	1
318.9	6.8(3)	0.83(2)	$9^- \rightarrow 7^-$	1
322.4	105.0(10)	0.73(1)	$2^+ \rightarrow 0^+$	Y
336.3	3.7(4)	0.68(3)	$13^- \rightarrow 12^-$	1
371.8	3.0(2)	0.70(4)	$14^- \rightarrow 13^-$	1
387			$(14^+) \rightarrow 14^+$	5 →Y
394.7	2.5(2)	0.60(7)	$15^- \rightarrow 14^-$	1
396	1.0(2)	0.59(4)	$3^+ \rightarrow 2^+$	γ
416.6	7.1(3)	0.75(4)	$10^- \rightarrow 8^-$	1
417	<0.5		$5^+ \rightarrow 4^+$	γ
420.8	1.7(2)	0.67(9)	$16^- \rightarrow 15^-$	1
440.1	1.1(2)	0.74(8)	$17^- \rightarrow 16^-$	1
458.9	0.6(1)	0.94(10)	$8^- \rightarrow 6^-$	3
462.5	0.7(2)	0.70(10)	$18^- \rightarrow 17^-$	1

TABLE 3—continued

E_γ	I_γ	DCO ratio	Assigned $I_i \rightarrow I_f$	Band
472.7	<1.0		$8^- \rightarrow 7^-$	$1 \rightarrow 2$
473.5	100.0	0.83(2)	$4^+ \rightarrow 2^+$	Y
476	3.3(4)	0.81(8)	$9^- \rightarrow 7^-$	2
476	<0.5		$3^+ \rightarrow 4^+$	$\gamma \rightarrow$ Y
480.1	0.7(2)		$19^- \rightarrow 18^-$	1
481.1	1.4(2)	0.87(6)	$(12^+) \rightarrow 12^+$	5→Y
499.3	7.6(3)	0.82(3)	$11^- \rightarrow 9^-$	1
500	< 1	0.6(2)	$(20^-) \rightarrow 19^-$	1
507.5	0.8(2)	0.54(7)	$8^- \rightarrow 7^+$	$1 \rightarrow \gamma$
507.7	0.5(1)	0.37(5)	$8^- \rightarrow 7^-$	3→2
525.2	3.2(3)	0.70(5)	$4^+ \rightarrow 2^+$	γ
532.2	2.5(1)	0.87(7)	$10^- \rightarrow 8^-$	3
545.5	4.2(2)	0.80(3)	$5^+ \rightarrow 3^+$	γ
553.6	3.7(3)	0.60(10)	$2^+ \rightarrow 2^+$	$\gamma \rightarrow$Y
564.4	1.0(2)	0.30(3)	$10^- \rightarrow 9^-$	3→2
573.5	6.3(2)	0.90(4)	$12^- \rightarrow 10^-$	1
576	0.2(1)		$12^- \rightarrow 11^-$	3→2
585.1	5.5(4)	0.75(5)	$6^+ \rightarrow 4^+$	γ
589	< 1		$6^+ \rightarrow 6^+$	$\gamma \rightarrow$Y
592.6	2.5(3)	0.97(9)	$12^+ \rightarrow 10^+$	4
601.5	86.7(10)	0.90(2)	$6^+ \rightarrow 4^+$	Y
605.2	4.0(5)		$4^+ \rightarrow 4^+$	$\gamma \rightarrow$Y
621.0	10.5(4)	0.95(3)	$11^- \rightarrow 9^-$	2
632.1	3.7(1)	0.90(10)	$12^- \rightarrow 10^-$	3
637	0.5(1)		$(12^-) \rightarrow (10^-)$	6
643.8	3.5(4)	1.03(5)	$7^+ \rightarrow 5^+$	γ
644.3	4.0(4)	0.83(6)	$13^- \rightarrow 11^-$	1
656.2	1.2(3)	0.53(11)	$6^- \rightarrow 5$	1→
657.5	0.7(1)	0.90(13)	$13^- \rightarrow 11^-$	2→1
668.2	4.9(4)	0.85(10)	$8^+ \rightarrow 6^+$	γ
672.4	2.6(3)	0.83(11)	$10^+ \rightarrow 8^+$	$4 \rightarrow \gamma$
690			$(14^+) \rightarrow (12^+)$	5
690.0	4.0(3)	1.12(10)	$14^+ \rightarrow 12^+$	4
702	<1		$13^- \rightarrow 11^-$	1→2
702.3	54.2(8)	0.97(2)	$8^+ \rightarrow 6^+$	Y
705	<0.4		$(13^-) \rightarrow (11^-)$	6
707.7	5.1(4)	1.00(5)	$14^- \rightarrow 12^-$	1
713.6	2.2(4)	1.05(6)	$9^+ \rightarrow 7^+$	γ

TABLE 3—continued

E_γ	I_γ	DCO ratio	Assigned $I_i \rightarrow I_f$	Band
714.9	11.8(5)	1.08(5)	$13^- \rightarrow 11^-$	2
719.5	2.4(4)	0.65(6)	$11^- \rightarrow 10^+$	2→Y
721.0	2.8(3)	1.00(6)	$14^- \rightarrow 12^-$	3
726			$(14^-) \rightarrow (12^-)$	6
732.4	0.3(1)		$7^- \rightarrow 8^+$	1→Y
742.6	0.4(1)	0.85(9)	$6^- \rightarrow 6^+$	1→ γ
759.8	2(1)	1.02(9)	$11^+ \rightarrow 9^+$	γ
762			$(13^+) \rightarrow 11^+$	γ
766.5	3.4(2)	0.95(6)	$15^- \rightarrow 13^-$	1
773.6	43.0(8)	1.00(2)	$10^+ \rightarrow 8^+$	Y
773.6			$16^+ \rightarrow 14^+$	Y
779.4	8.1(4)	1.05(4)	$15^- \rightarrow 13^-$	2
782.7	14.5(10)	1.03(3)	$14^+ \rightarrow 12^+$	Y
789.8	1.2(3)	1.10(10)	$(16^+) \rightarrow (14^+)$	5
792.7	0.3(1)	0.81(16)	$15^- \rightarrow 13^-$	2→1
797.5	3.0(3)	0.98(5)	$16^+ \rightarrow 14^+$	4
803.3	2.4(3)	0.98(7)	$16^- \rightarrow 14^-$	3
804.1	24.5(4)	1.00(2)	$12^+ \rightarrow 10^+$	Y
815.1	2.6(2)	1.20(10)	$16^- \rightarrow 14^-$	1
818.7	7.2(3)	0.99(3)	$18^+ \rightarrow 16^+$	Y
820	1.1(2)		$(18^+) \rightarrow (16^+)$	5
844.2	5.7(3)	1.00(8)	$17^- \rightarrow 15^-$	2
860.9	2.9(3)	0.97(6)	$17^- \rightarrow 15^-$	1
864	<1		$(20^+) \rightarrow (18^+)$	5
872.3	10.7(3)	0.55(2)	$9^- \rightarrow 8^+$	2→Y
876.0	1.2(2)		$2^+ \rightarrow 0^+$	γ →Y
882.7	1.7(2)	1.00(10)	$18^- \rightarrow 16^-$	3
902.8	0.8(2)	1.04(7)	$18^- \rightarrow 16^-$	1
904.4	3.2(3)	1.00(4)	$20^+ \rightarrow 18^+$	Y
904.5	1.0(1)	0.89(6)	$8^- \rightarrow 8^+$	3→Y
904.6	3.5(2)	0.89(6)	$19^- \rightarrow 17^-$	2
911.9	0.5(2)	0.52(12)	$6^- \rightarrow 5^+$	1→ γ
932	<1		$14^+ \rightarrow 12^+$	4→Y
933	1.5(5)	0.92(11)	$18^+ \rightarrow 16^+$	4
937.3	1.1(1)	0.90(15)	$20^- \rightarrow 18^-$	3
942.6	1.4(3)	1.11(12)	$19^- \rightarrow 17^-$	1
949.6	2.5(3)		$3^+ \rightarrow 2^+$	γ →Y
955	0.7(1)	0.96(10)	$22^- \rightarrow 20^-$	3

TABLE 3—continued

E_γ	I_γ	DCO ratio	Assigned $I_i \rightarrow I_f$	Band
965.0	2.3(3)	1.02(9)	$21^- \rightarrow 19^-$	2
980	1.4(5)		$(20^-) \rightarrow 18^-$	1
981	0.6(2)		$(20^+) \rightarrow 18^+$	5→4
999.7	1.8(2)	1.01(7)	$22^+ \rightarrow 20^+$	Y
1011.7	1.3(3)		$(23^-) \rightarrow 21^-$	2
1014	1.9(5)		$(21^-) \rightarrow 19^-$	1
1016	<0.5		$(24^-) \rightarrow 22^-$	3
1022	2.6(4)		$5^+ \rightarrow 4^+$	$\gamma \rightarrow$Y
1046.1	2.7(3)	0.80(15)	$12^+ \rightarrow 10^+$	4→Y
1064.0	1.0(3)		$7^+ \rightarrow 6^+$	$\gamma \rightarrow$Y
1065	0.5(1)		$(25^-) \rightarrow (23^-)$	2
1075	<0.5		$9^+ \rightarrow 8^+$	$\gamma \rightarrow$Y
1079	0.20(7)		$4^+ \rightarrow 2^+$	$\gamma \rightarrow$Y
1088			$(20^+) \rightarrow 18^+$	4
1096	0.7(2)	1.01(13)	$24^+ \rightarrow 22^+$	Y
1098.7	8.1(3)	0.62(1)	$7^- \rightarrow 6^+$	2→Y
1127	<0.5		$(27^-) \rightarrow (25^-)$	2
1147	<0.5		$(29^-) \rightarrow (27^-)$	2
1147.8	0.6(1)	0.85(5)	$6^- \rightarrow 6^+$	3→Y
1160	0.2(1)		$(26^-) \rightarrow (24^-)$	3
1170.8	1.4(2)	1.2(2)	$(14^+) \rightarrow 12^+$	5→Y
1178.0	1.2(2)	1.0(2)	$(16^+) \rightarrow 14^+$	5→Y
1190	<1		$(26^+) \rightarrow 24^+$	Y
1225	0.7(3)		$(18^+) \rightarrow 16^+$	5→Y
1268.6	0.8(3)	0.66(8)	$5 \rightarrow 4^+$	$6 \rightarrow \gamma$
1276.9	2.2(2)	0.49(5)	$5 \rightarrow 4^+$	→Y
1283	<0.5		$(28^+) \rightarrow (26^+)$	Y
1285.2			$(12^+) \rightarrow 10^+$	5→Y
1434.8	10.0(5)	0.53(4)	$7^- \rightarrow 6^+$	1→Y
1516	0.7(2)		$\rightarrow 6^+$	→Y
1533.7	3.2(3)	0.63(6)	$7^- \rightarrow 6^+$	→Y

obtained for the 672.4 keV transition connecting band 4 to the γ-band, as well as for the four lowest transitions in band 4, are consistent with a $\Delta I = 2$ quadrupole character resulting in the spin and parity assignments shown in Fig. 5. Our spin assignments are also supported by the DCO ratios measured for the 149.2 and 242.0 keV transitions connecting band 5 to the yrast band. Note, that in subsect. 3.2 we reported a very similar

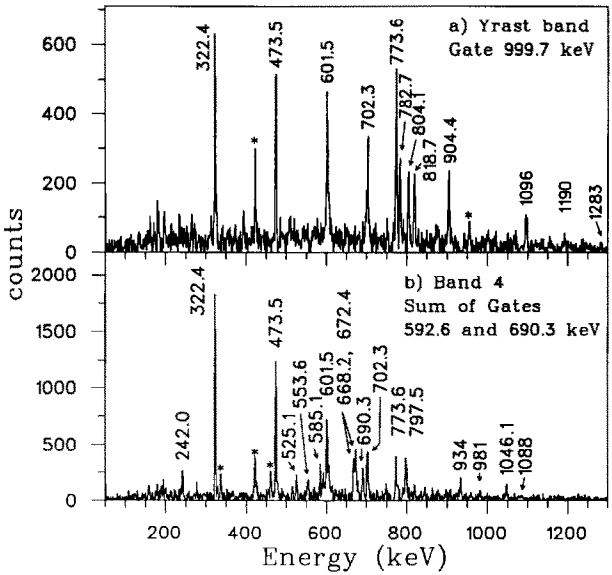

Fig. 6. Sample coincidence spectra from the ^{106}Pd(^{18}O,4n)^{120}Xe reaction. The peaks labelled by energy are placed in the ^{120}Xe level scheme. Peaks labelled with an asterisk are due to contaminants.

band in ^{118}Xe.

A weakly populated cascade of γ-rays, band 5, was also observed. The states of this band feed the $I^{\pi} = 10^{+} - 16^{+}$ yrast states. The DCO ratios for the connecting 481.1, 1170.8 and 1178.0 keV transitions suggest positive parity and even spins for band 5.

Rouabah et al. [11] have reported a band built on a 10^{+} state at 2631 keV. In ref. [15] this band was extended by two new transitions, and the band head was changed to 8^{+}. Our data show that this band was incorrectly placed in the level scheme, see Fig 7. We observed a cascade of γ-rays (band 3), including the transitions observed in refs. [11,15], forming a band built on a 6^{-} state at 2545 keV. This band is connected to another negative-parity band (band 2) by three transitions. The very small DCO ratios (≈ 0.3) deduced for these transitions, are consistent only with $\Delta I = 1$ transitions having negative E2/M1 mixing ratios. Band 2 was previously known to the 29^{-} state [11,15]. In the present work the transitions previously assigned to this band could be confirmed.

Band 1, consisting of intense $\Delta I = 1$ transitions and stretched quadrupole transitions was extended to $I^{\pi} = (21^{-})$. At the bottom of this band several new transitions were placed, and the decay to the ground band was found to be complicated (Fig. 5). The indicated 38 and 56 keV transitions from the 8^{-} state at 2969 keV could not be directly observed in the γ-ray spectra; their existence is, however, clear from the coincidence relations between other γ-rays. The 6^{-} and 7^{-} assignments for the states at 2729 and 2832 keV, respectively, result from the observation of several transitions with a stretched dipole character between these states and other known states.

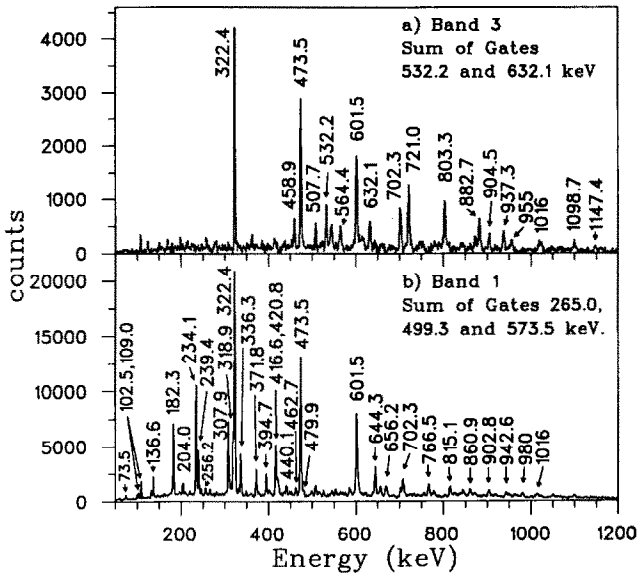

Fig. 7. Sample coincidence spectra for ^{120}Xe. The peaks labelled by energy are placed in the ^{120}Xe level scheme. Peaks labelled with an asterisk are due to contaminants.

In the coincidence spectra, gated on the lowest transitions in band 1, additional transitions (see Fig. 7) are present which neither belong to band 1 nor to the decay out of band 1. These γ-rays indicate the existence of a new band, band 6. However, only a few intraband transitions are observed. Band 6 and band 1 seem to interact strongly, because intense interband transitions are observed.

The odd-spin members of band 1 lie very close in energy to the states with the same spin values in band 2. Bands 1 and 2 apparently cross each other first at $I^\pi = 13^-$ and again above $I^\pi = 17^-$. As a signal of the crossing and the interaction, interband transitions are observed. The measured intraband/interband branching ratios are used in subsect. 4.2.6 to extract the interaction strength between bands 1 and 2.

4. Discussion

One aim of nuclear structure studies is to understand the interplay between the collective and single-particle degrees of freedom. In recent years a great deal of interest has been focused on transitional nuclei. The Xe-nuclei have been described within the context of IBA in large detail [2]. In the present paper we will mainly compare our experimental results with mean-field calculations. Since rotation is one of the most powerful tools to reveal the single-particle structure of different excitation modes, we also address the question, to what extent different models are capable of tracing sudden changes in the internal structure.

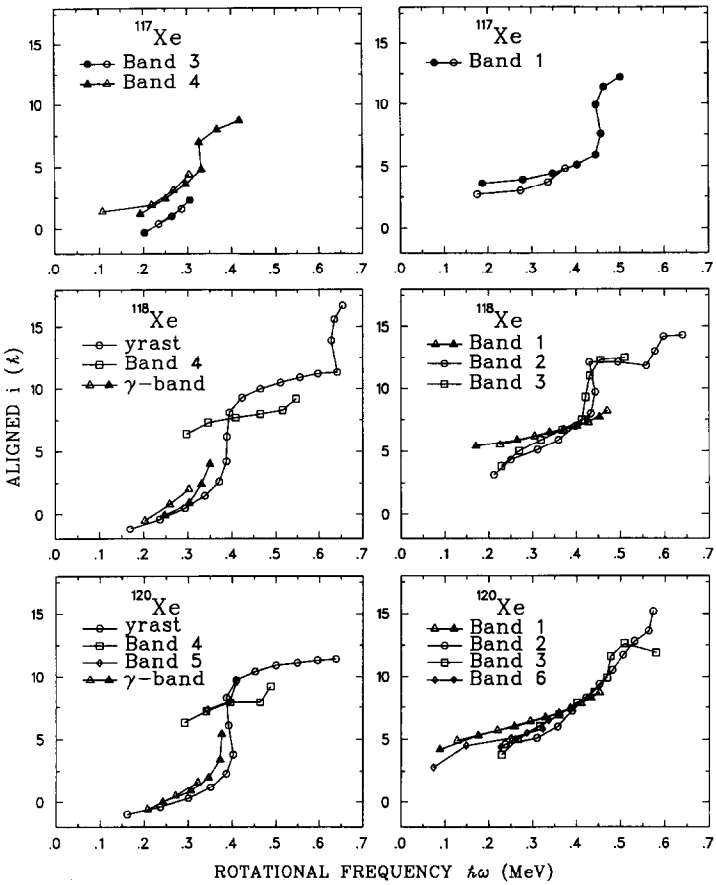

Fig. 8. Alignments for various bands in ^{117}Xe, ^{118}Xe and ^{120}Xe. A reference configuration with parameters $J_0 = 15\hbar^2\text{MeV}^{-1}$ and $J_1 = 25\hbar^4\text{MeV}^{-3}$ has been subtracted.

In order to compare the theoretical prediction with the experimental data in ^{117,118,120}Xe, aligned angular momenta and routhians were extracted according to ref. [23]. These quantities are plotted in Figs. 8 and 9 as a function of the rotational frequency.

The alignment in the yrast sequence of the even Xe-isotopes is shown in Fig. 10. Obviously, there is a major change when going from ^{120}Xe to ^{122}Xe. Similar sudden changes are observed in the excited bands and will be addressed more in detail in the following.

4.1. TOTAL ROUTHIAN SURFACE CALCULATIONS

Total routhian surface (TRS) calculations for this mass region have been performed by Wyss et al. [24] using a Woods–Saxon potential and a monopole pairing residual

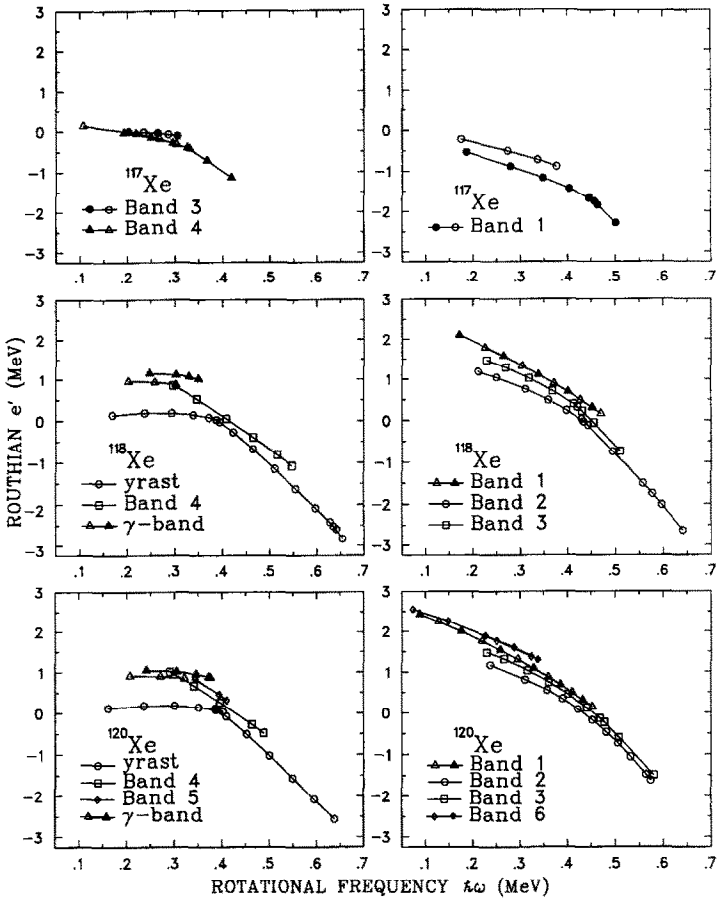

Fig. 9. Routhians for various bands in ^{117}Xe, ^{118}Xe and ^{120}Xe.

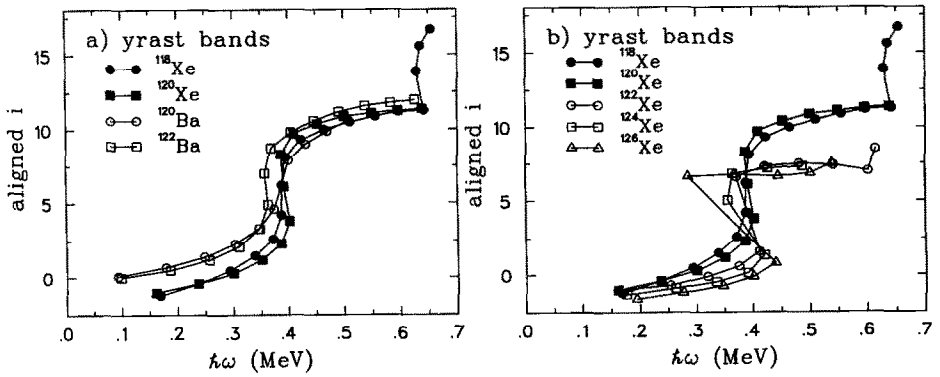

Fig. 10. Aligned angular momenta of the yrast bands in ^{118}Xe and ^{120}Xe compared with (a) the neighbouring even Ba-nuclei and (b) the heavier even Xe-nuclei.

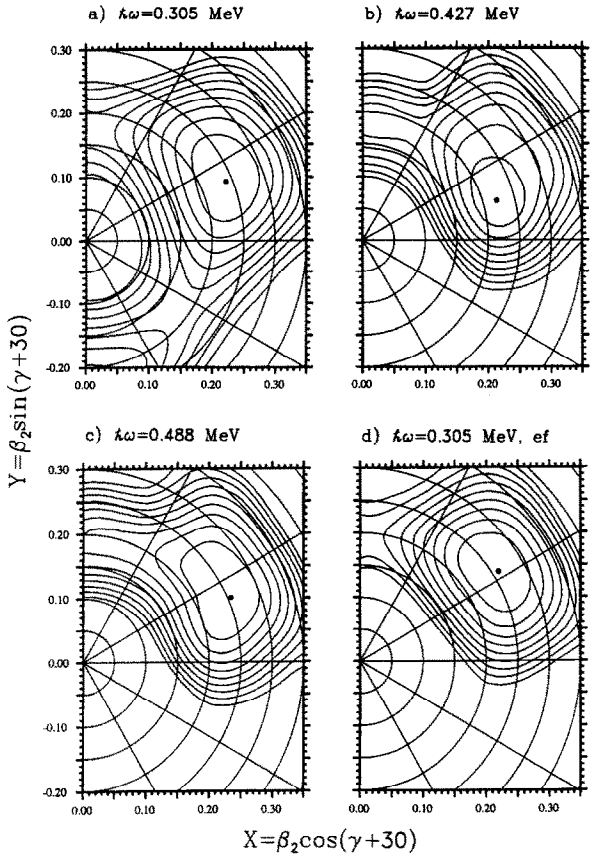

Fig. 11. A sample TR surfaces for ^{118}Xe. (a), (b) and (c) show the vacuum configuration, while (d) shows the proton ef configuration.

interaction. In the following text we have adopted a commonly used notation for labelling the TR surfaces [9]. The lowest positive-parity (negative-parity) neutron and proton configurations are denoted by A, B,... (E, F,...) and a, b,... (e, f,...), respectively. The association of the calculated surfaces with the quasiparticles is straightforward for the negative-parity configurations, since the $h_{11/2}$ orbital has a unique parity in this mass region. The aligned $(h_{11/2})^2$ configuration is then labelled by EF (ef) for neutrons (protons). For the positive-parity 1qp configurations the surfaces are composed of the $\frac{3}{2}^+[411]$, $\frac{5}{2}^+[413]$, $\frac{1}{2}^+[411]$ and $\frac{5}{2}^+[402]$ Nilsson states for the neutrons, and of the $\frac{1}{2}^+[420]$, $\frac{3}{2}^+[422]$ and $\frac{9}{2}^+[404]$ states for the protons. For reason of simplicity, we will also use the spherical labels $g_{7/2}$, $d_{5/2}$ etc., from which the Nilsson states originate.

Some examples of TR surfaces for the yrast ($\pi = +, \alpha = 0$) configuration in ^{118}Xe are shown in Figs. 11a–c. At a rotational frequency of 0.305 MeV the surface represents the g.s. band, and the calculation indicates a shape with $\beta_2 = 0.24$ and a slightly negative

γ-deformation. The surface is stiffer than in the heavier Xe-isotopes. At the frequency 0.427 MeV the position of the energy minimum is shifted to $\beta_2 = 0.22$ and $\gamma = -13.7°$, while at a frequency of 0.487 the minimum is at $\beta_2 = 0.26$ and $\gamma = -6.6°$. The frequencies for these two surfaces are just above the neutron EF and proton ef alignments, respectively. The shifts in the deformation parameters reflect the different shape-driving tendencies of the neutron and proton $(h_{11/2})^2$ configurations. The two-quasiparticle proton $(h_{11/2})^2$ configuration solely, as shown in Fig. 11d, drives the nucleus to $\beta_2 \approx 0.26$ and $\gamma > 0°$. From the calculations, we can thus conclude that aligned protons and neutrons prefer different shapes and that the angular momentum alignment will strongly be connected to the evolution of the shape.

The results from the TRS calculations for $^{117-120}$Xe are collected in Table 4, where the predicted shapes (β_2, β_4, γ) and the first neutron and proton $(h_{11/2})^2$ alignment frequencies are listed. The predictions for the nucleus ^{119}Xe are included for completeness. The predicted quadrupole deformations vary between 0.22 and 0.28 depending on the configuration. The shapes for the related configurations in ^{117}Xe and ^{119}Xe, as well as in ^{118}Xe and ^{120}Xe, are quite similar. The frequency of the proton $(h_{11/2})^2$ alignment depends very sensitively on both β_2 and γ [1]. The Fermi surface for protons lies below the $\Omega = \frac{1}{2}$, $h_{11/2}$ orbital. Therefore, an increasing quadrupole deformation and more positive values of γ lower the frequency of this alignment. The gain in the aligned angular momentum according to the TRS calculations is about $7\hbar$ each for the neutron and proton $(h_{11/2})^2$ alignments, respectively. The deformation systematics of the even Xe-isotopes has been discussed in ref. [1]. They show that softness of the potential-energy surface increases with N, leading to a transition from preferably prolate to oblate and strongly triaxial shapes. This shape transition occurs in the g.s. band when going from ^{126}Xe to ^{128}Xe and in the neutron S-band when going from ^{120}Xe to ^{122}Xe [1]. We believe that these shape changes are the key to the understanding of the very different excitation pattern in the Xe-isotopes with increasing neutron number.

4.2. PROPERTIES OF ROTATIONAL BANDS IN ^{118}Xe AND ^{120}Xe

4.2.1. Positive-parity yrast bands. The alignment plots (Fig. 8 and 10b) for ^{118}Xe and ^{120}Xe look in many respects similar. The first band crossing in the g.s. band occurs at $\hbar\omega = 0.39$ MeV, and the increase in the alignment is about $10\hbar$. The next jump in the alignment plot for the yrast band in ^{118}Xe takes place at $\hbar\omega = 0.62$ MeV. In an earlier paper [16] we interpreted this alignment gain as a sign of a transition to a terminating band structure.

In this mass region the first band crossing has usually been attributed to the $h_{11/2}$ neutrons [10,11]. However, the aligned angular momentum above the band crossing in the yrast band is somewhat larger than what could be expected from the initial alignments in the $h_{11/2}$ band in ^{117}Xe, see subsect. 4.3 below. Furthermore, the observed band crossing at $\hbar\omega = 0.45$ MeV in this band gives due to a less favourable shape an upper limit for the proton $(h_{11/2})^2$ alignment frequency in the g.s. bands of neighbouring even Xe-nuclei.

TABLE 4

Results from the TRS calculations. The deformation parameters are given at $\hbar\omega = 0.305$ MeV

	Deformation				First alignment	
nucleus	configuration	β_2	β_4	γ	conf.	$\hbar\omega$(MeV)
^{117}Xe	A	0.245	0.038	−1.7	EF	0.34
	B	0.248	0.039	−3.7	EF	0.34
	E	0.221	0.024	−10.8	ef	0.45
	F	0.235	0.029	−3.4	ef	0.42
^{118}Xe	g.s. band [a]	0.224	0.021	−0.2		
	g.s. band	0.240	0.029	−7.2	EF	0.34
	EF	0.222	0.013	−8.3	ef	0.46
	ef	0.260	0.035	2.4		
	ea	0.228	0.039	10.3	EF	0.34
	eb	0.225	0.038	13.0	EF	0.34
	ec	0.240	0.030	5.4	EF	0.35
	ed	0.259	0.034	2.6	EF	0.39
	EA	0.229	0.022	−12.0	ef	0.46
	EB	0.230	0.017	−6.1	ef	0.46
^{119}Xe	A	0.253	0.025	−8.4	EF	0.34
	B	0.247	0.021	−2.1	EF	0.34
	E	0.225	0.014	−12.0	FG and ef	0.45
	F	0.235	0.014	−4.6	ef and EH	0.45
^{120}Xe	g.s. band [a]	0.224	0.012	−0.1		
	g.s. band	0.241	0.014	−5.5	EF	0.34
	EF	0.217	0.003	−8.3	ef	0.46
	ef	0.265	0.020	3.8		
	ea	0.232	0.027	10.1	EF	0.35
	eb	0.227	0.026	12.9	EF	0.35
	ec	0.241	0.018	6.2	EF	0.35
	ed	0.260	0.020	4.7	EF	0.39
	EA	0.22	0.019	−16.4	FG	≈0.45
	EB	0.22	0.004	−6.2	FG	≈0.45

[a] At $\hbar\omega = 0.00$ MeV.

The proton $\frac{1}{2}^-[550]$ bands in ^{119}Cs and ^{121}Cs experience smooth neutron alignments at $\hbar\omega = 0.45$ MeV [5]. In the $\frac{1}{2}^-[550]$ band in ^{117}I the alignment is increasing even more smoothly from the bottom of the band up to the last observed $\frac{43}{2}^- \rightarrow \frac{39}{2}^-$ transition without any apparent sign of the neutron $h_{11/2}$ alignment [25]. The lack of an apparent band crossing around $\hbar\omega = 0.4$ MeV might be explained with a very large interaction between the particle-like proton $\frac{1}{2}^-[550]$ configuration and the aligning $h_{11/2}$ neutrons [26]. However, in ref. [27] an indication of upbend at $\hbar\omega \approx 0.5$ MeV is observed, which also might be connected to non-collective states.

In Fig. 10 the experimental aligned angular momentum curves for the yrast bands of ^{118}Xe and ^{120}Xe are compared to those of the neighbouring Ba-nuclei and the heavier Xe-

nuclei. As can be seen from Fig. 10a, the aligned angular momenta above the first band crossing are almost identical for the Xe- and Ba-nuclei shown. In the ^{120}Ba- and ^{122}Ba-nuclei the band crossing in the g.s. band is explained as the alignments of the $h_{11/2}$ protons (at $\hbar\omega = 0.35$ MeV) and subsequently of the $h_{11/2}$ neutrons (at $\hbar\omega = 0.45$ MeV) [6,28], where the yrast–yrare interaction for the $\nu(h_{11/2})^2$ configuration is very large (see the previous discussion for the Cs- and I-isotopes). In the even Xe-nuclei with $A \geqslant 122$ [29–32] the aligned angular momenta above the first band crossing reach a value of about $7\hbar$, see fig 10b. In these nuclei the first band crossing in the yrast band is attributed to the $h_{11/2}$ neutrons only. When going from ^{122}Xe to ^{120}Xe and ^{118}Xe we observe a sudden increase of about 3–$4\hbar$ in the aligned angular momentum. Such an increase in the aligned angular momentum is unexpected if one deals with the neutron $(h_{11/2})^2$ configuration only.

The data shown in Fig. 10 strongly suggest that the observed band crossing in the yrast bands of ^{118}Xe and ^{120}Xe at $\hbar\omega = 0.39$ MeV involves not only the neutron $h_{11/2}$ alignment but also the proton $h_{11/2}$ alignment, similar to the situation in ^{120}Ba and ^{122}Ba. Differing from the Ba-nuclei, the neutron and proton $h_{11/2}$ alignments seem to occur at about the same rotational frequency.

According to the TRS calculations for ^{118}Xe, the neutron EF and proton ef bands cross the g.s. band at $\hbar\omega = 0.34$ and 0.42 MeV, respectively. The EF band experiences the proton $(h_{11/2})^2$ alignment at $\hbar\omega = 0.46$ MeV. For ^{120}Xe the TRS calculations give similar results. Note however, that due to the approximative treatment of pairing in the TRS calculations, extracted crossing frequencies are somewhat uncertain. In the case of the Xe-nuclei, additional difficulties arise through the strong dependence of the crossing frequency on deformation. As discussed previously and more in detail in ref. [1], an increased β_2 deformation lowers (delays) the proton (neutron) crossing. The TRS calculations indicate a stretching in the g.s. band from $\beta_2 = 0.224$ at $I = 0$ to $\beta_2 = 0.246$ at $I \approx 8$. This stretching of the nucleus in the course of rotation leads to a change in the single-particle structure, in particularly of the protons, where the occupation probabilities for the $\frac{9}{2}^+[404]$ and $\frac{1}{2}^+[420]$ states decreases while it increases for the $\frac{1}{2}^-[550]$ state. Since the band-crossing frequency and deformation are intimately linked, small differences will easily reverse the order of the calculated proton and neutron crossing frequency. Besides the uncertainties connected with pairing and deformation, the neutron crossing frequency in the CSM calculations is undoubtedly too low when compared to experiment. Similar observations in the rare-earth region have been attributed to the presence of quadrupole pairing correlations [33].

4.2.2. The γ-vibrational bands. The γ-vibrational bands in Xe-isotopes are characterized by low excitation energy. In the TRS calculations, this is reflected by a γ-soft potential-energy surface. In our RPA calculation a typical zero-point amplitude of the γ degree of freedom is 20°. The structure of the γ-band at high spin has been a long standing problem. The possible occurrence of a γS-band, i.e. a vibrational band coupled to an aligned pair of quasiparticles, has been addressed for the first time in microscopical calculations for the Er-isotopes [34]. Later on, the observed continuation of the γ-bands

in ^{182}Os and ^{126}Ba, both of which carry aligned angular momenta, have been interpreted in terms of a wobbling motion [35,36]. On the other hand, the lack of strong interband transitions implies that there is no firm experimental evidence for a wobbling motion. We expect that the γ-softness of the Xe-isotopes may offer an opportunity for identifying a γS-band, for which there are several candidates in ^{118}Xe and ^{120}Xe. In both nuclei, the $\alpha = 0$ signature of the γ-band is crossed at $I = 10$ by an aligned configuration. The crossing frequency is remarkably low, $\hbar\omega \approx 0.30$ MeV. The crossing band, band 4, feeds both the yrast band and the γ-band. The $\alpha = 1$ sequence of the γ-band experiences a band crossing at a higher frequency of $\hbar\omega \approx 0.38$ MeV. In addition, another aligned $(+,0)$ band is observed in ^{120}Xe, band 5. In the heavier Xe-isotopes, instead of the $\alpha = 0$ sequence, it is the $\alpha = 1$ sequence of the γ-band which continues to high spin.

First, we study the character of band 4. The low excitation energy of only 150 (255) keV of band 4 in ^{120}Xe (^{118}Xe) relative to the yrast band suggests that this structure is more of pure 2qp character, and less of collective nature, i.e. not a γS-band. The systematics of the yrast band crossing properties further supports this interpretation: Band 4 crosses the extrapolated g.s. band at $\hbar\omega = 0.41$ MeV in ^{118}Xe and at $\hbar\omega = 0.43$ MeV in ^{120}Xe. These crossings take place only at a slightly higher frequency than the first crossings in the yrast band (c.f. Figs. 8 and 9). The aligned angular momentum for band 4 in ^{118}Xe and ^{120}Xe is 7–8$\hbar$. This is similar to that found for the neutron S-bands in heavier even Xe-nuclei, where the crossing frequency is compatible with the systematics (see Fig. 6 in ref. [1]). The character of the $\Delta I = 0$ transitions between band 4 and the yrast band is M1-like in ^{120}Xe, while in ^{118}Xe the data are not conclusive. Note that the $B(\mathrm{M1};I \rightarrow I)$ rates from the γ-band to yrast band should be retarded, and the observation of dominant M1-transitions (DCO ≈ 1.1) in ^{120}Xe is another sign of band 4 being a 2qp configuration.

The preferred negative γ-value and rather low β_2-deformation of the $h_{11/2}$ neutron 2qp configuration might lead to large overlap with the γ-band and could account for the low-lying crossing frequency. We thus assign, in agreement with ref. [1], band 4 as a shape-coexisting neutron S-band, and not as the γS-band. This situation is in fact analogous to the crossing in the β-band in ^{156}Dy [37]. There, the aligned S-band has a larger quadrupole deformation than the vacuum, due to the occupation of the previously non-occupied $i_{13/2}$ neutrons, and it has larger overlap with the β-band than with the g.s. band. Low-lying band crossings in the vibrational bands may thus many times be associated with coexisting shapes, which couple to the vibrational motion.

There are some differences between bands 4 in ^{118}Xe and ^{120}Xe. The decay pattern from the neutron S-band to the mixed $h_{11/2}$ proton–neutron 4qp yrast band yields strong $I \rightarrow I$ interband transitions in both nuclei, however, in ^{118}Xe they involve the 10^+ and 12^+ states, whereas they connect the 12^+ and 14^+ states in ^{120}Xe. In ^{120}Xe one observes in addition $I \rightarrow I - 2$ interband transitions, which however are rather weak (in B(E2)'s), see Fig. 12. The decay properties may be understood in terms of the occupation of the $\pi h_{11/2}$ orbital: With increasing mixing of the $(h_{11/2})^2$ aligned protons into the yrast sequence, the difference between band 4 and the yrast sequence will increase, yielding reduced interband transitions. Therefore, the differences in the decay pattern between

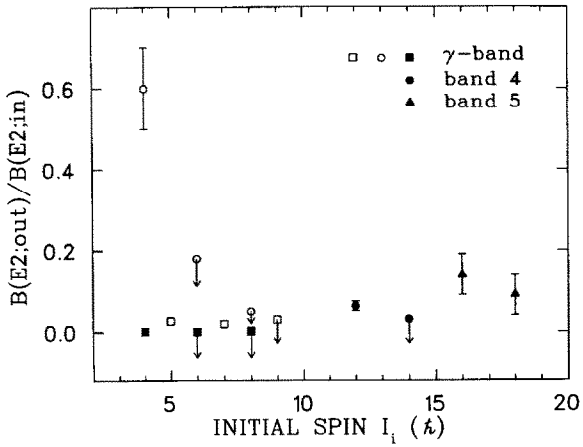

Fig. 12. Interband/intraband B(E2) branching ratios of E2 transitions in ^{120}Xe. The filled symbols show the branching ratios of the stretched E2 transitions for band 4 (•), band 5 (▲) and the γ-band (■). The open symbols show the B(E2) ratios for the γ-band, when the interband transition is of the $\Delta I = 0$ (○) or the $\Delta I = 1$ (□) type. The $\Delta I = 0, 1$ transitions to the g.s. band are assumed to be of the E2 character.

^{118}Xe and ^{120}Xe might be related to a somewhat earlier onset of the alignment and a larger interaction strength in ^{118}Xe as compared to ^{120}Xe.

Another candidate for a γS-band is band 5 in ^{120}Xe. An interesting property of this band are the strong $\Delta I = 2$ branchings to the yrast band; $B(\mathrm{E2}: 5 \rightarrow \mathrm{yrast})/B(\mathrm{E2}: 5 \rightarrow 5)$ are about 0.1. This indicates a band built on a collective excitation mode. Looking at the alignment curve (Fig. 8) closely, the $16^+ - 14^+ - 12^+$ sequence is almost parallel to that in band 4, and in addition, band 5 begins to upbend at the same frequency as the yrast band. Although the 10^+ state is missing, these properties seem to indicate that band 5 is the $\alpha = 0$ signature of the γS-band. The γ-band would thus experience the first band crossing (neutron $h_{11/2}$) at 0.34 MeV and the second one (proton $h_{11/2}$) at 0.4 MeV. The difference in the first crossing frequency to the yrast band may be attributed to the property that the γ-band is effectively more triaxial than the yrast band. The crossing frequency in the $\alpha = 1$ sequence is situated intermediate between the $\alpha = 0$ sequence of the γ-band and the yrast band. Indeed, our RPA calculations show that there are γ-vibrational excitations built not only on the neutron 2qp but also on the neutron–proton 4qp configuration. This implies that for the first time one might observe a γS-band, built upon a 4qp aligned configuration.

It is interesting to note that in ^{122}Xe the yrast band is built upon the $h_{11/2}$ neutrons alone and the corresponding continuation of the γ-band is not observed. With increasing N, the odd-spin members of the γ-bands come lower in energy and in particular, in ^{124}Xe, it is this branch in which a band crossing has been observed. A possible explanation for the change of the γ-band might be the shape change towards increased triaxiality: Not only the yrast configuration changes its shape gradually, but also the neutron 2qp configuration changes

shape between $A = 120$ and 122 (see Fig. 3 in ref. [1]). Indeed, the observed odd-spin sequence of the γS-band in ^{124}Xe is reproduced very well within the RPA calculations adopting $\beta = 0.20$ and $\gamma = -45°$. This RPA solution has well developed wobbling character: (a) its routhian is an increasing function of the frequency, (b) it shows the asymmetric-rotor-model-like moments of inertia, and (c) its wave function is strongly K-mixed. These properties vary very smoothly with γ and/or N. Therefore, we can expect that this wobbling-like excitation exists also in neighbouring nuclei, as for example, in ^{122}Xe.

The rotational pattern of the light Xe-isotopes thus suggest large structural changes. The Xe-isotopes have also been described in the framework of IBA in terms of O(6) character [38]. For the γ-band, this implies essentially similar magnitude of the transition rates of the $I \rightarrow I$ interband and $I \rightarrow I - 2$ intraband transitions. While this might hold for the very low-spin part of the γ-band in the Xe-isotopes, it is definitively not true at higher spins, since no transitions to the g.s. band were detected above spin 6, see Fig. 12. This further implies that the structural content of the g.s. band and the γ-band develop differently with spin. As discussed previously, the proton structure is changing gradually in the g.s. band. Taking into account the spread in γ and the smaller β_2 values of the γ-band, the proton "two-particle–two-hole" excitation is present to a much smaller extent in the structure of the γ-band, hence yielding, with increasing spin, reduced interband transitions. Such changes of the internal structure seem to be outside the scope of the IBA-model.

4.2.3. Strongly coupled negative-parity bands. A set of negative-parity side bands are observed in the Xe-isotopes. These can be divided into two groups — one being strongly coupled, i.e. having very small signature splitting and decoupled sequences. The strongly coupled sequence has been observed in many Xe-isotopes but it is only governed by strong intraband B(M1) transition rates in $^{118-122}$Xe. There are only two configurations, with such strong B(M1) rate, namely the proton $g_{9/2}^{-1}h_{11/2}$ and neutron $d_{5/2}h_{11/2}$ configurations. For reasons of simplicity we use the label $g_{9/2}$ for the $\frac{9}{2}^+[404]$ and $d_{5/2}$ for the $\frac{5}{2}^+[402]$ Nilsson state. The positive sign of the mixing ratio δ clearly speaks in favour of the proton configuration, similar to the Ba-isotopes [28,36,39]. The properties of the strongly coupled band in ^{122}Xe [29] deviate from those of the $g_{9/2}^{-1}h_{11/2}$ bands in ^{118}Xe and ^{120}Xe and might be associated with the neutron 2qp configuration. Furthermore, another strongly coupled sequence has been observed in ^{122}Xe [30]. This sequence lacks M1 transitions and therefore it could originate from the neutron $g_{7/2}h_{11/2}$ configuration.

The change of the character of the side bands thus seems to indicate a change in the position of the $h_{11/2}$ proton configuration with respect to the $h_{11/2}$ neutrons. This can partly be understood by the deformation systematics of the Xe-nuclei as discussed in ref. [1]. With increasing N, the shape of the Xe-isotopes is calculated to become less deformed and more γ-soft, moving the $h_{11/2}$ proton subshell to higher energies. The 2qp excitation into the $g_{9/2}^{-1}h_{11/2}$ proton configuration is thus expected to become less favoured with N.

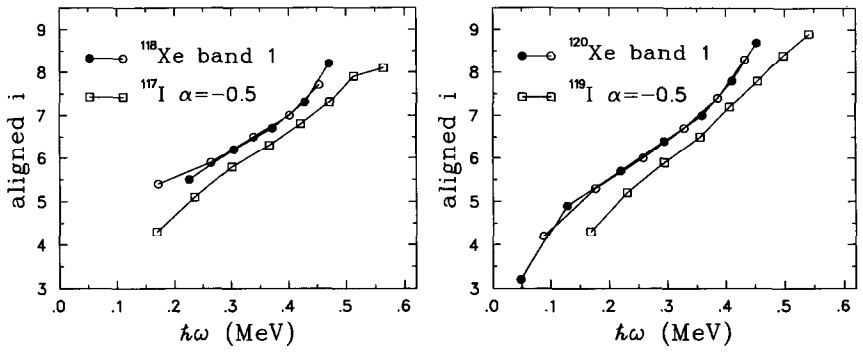

Fig. 13. Aligned angular momenta for the proton $g_{9/2}^{-1}h_{11/2}$ bands in ^{118}Xe and ^{120}Xe and for the proton $h_{11/2}$ bands in the iodine isotones.

The strongly coupled band 1 shows a very smooth alignment both in ^{118}Xe and in ^{120}Xe. In agreement with the $g_{9/2}^{-1}h_{11/2}$ configuration assignment, this band has a very large initial alignment (Fig. 8) reflecting the rotational properties of the proton $h_{11/2}$, $\frac{1}{2}^-[550]$ orbital. This band is extended to $\hbar\omega \approx 0.50$ MeV both in ^{118}Xe and in ^{120}Xe, but still we do not observe any clear sign of a band crossing. The slope of the alignment curve increases slightly around $\hbar\omega = 0.4$ MeV, which may be indicative of an alignment process. The increase of the $B(M1)/B(E2)$ ratios (c.f. Fig. 15) at the last data points also supports this picture. Band 6 in ^{120}Xe is associated with only a slightly smaller aligned angular momentum than band 1. Since this band is so strongly connected to band 1, it is also most likely based on the same quasiparticle configuration, but with a different K-value. Since the $\frac{9}{2}^+[404] \otimes \frac{1}{2}^-[550]$ configuration can couple to either $K = 4$ or $K = 5$, one expects two bands to be present close in energy. Note that the Coriolis force will mix the two bands strongly, yielding enhanced interband transitions, as seen in our data.

In Fig. 13 the aligned angular momenta of the $g_{9/2}^{-1}h_{11/2}$ bands in ^{118}Xe and ^{120}Xe are compared to those of the proton $h_{11/2}$ bands in ^{117}I [25] and ^{119}I [40]. The curves are nearly parallel, with the alignment being $\approx 0.5\hbar$ larger in the two-quasiproton bands than in the $h_{11/2}$ bands. Moreover, both of these bands increase their angular momenta smoothly up to $\hbar\omega \approx 0.40$ MeV, where the neutron $(h_{11/2})^2$ alignment is expected to occur. Evidently, the alignment properties of the $g_{9/2}^{-1}h_{11/2}$ bands in ^{118}Xe and ^{120}Xe are defined by the particle-like orbital, and the strongly coupled partner behaves as a spectator. The latter partner expresses itself in the intense intraband M1 transitions and the small signature splitting.

The very smooth alignment pattern in the light Cs-isotopes has been attributed to a residual np interaction [5]. For a quadrupole–quadrupole force, the residual np interaction affects the crossing frequency and the interaction between the crossing bands. The

lower the Fermi surface with respect to the high-j orbital, the larger is the calculated effect [41,42]. One therefore expects this interaction to increase slightly with decreasing proton number, e.g. when going to the light I-isotopes. The effect will be analogous for a 2qp configuration, i.e. proportional to the residual quadrupole moment of that configuration. The $g_{9/2}$ hole state has a positive quadrupole moment, i.e. will add to the positive quadrupole moment of the $h_{11/2}$ state, whereas the $\frac{1}{2}^+[420]$ or $\frac{3}{2}^+[431]$ state will decrease the residual quadrupole moment (as compared to the $h_{11/2}$ orbital alone). The residual np interaction will therefore more strongly smooth out the alignment in the $g_{9/2}^{-1}h_{11/2}$ configuration.

Due to the mixing of different configurations in one TR surface, one cannot always assign specific configurations to the extracted minima [9]. In the case of the ed configuration, one can assign the minimum above $\hbar\omega \geqslant 0.24$ MeV to the $g_{9/2}^{-1}h_{11/2}$ configuration. The ed configuration is highest in the calculation of the proton configurations. Three more proton configurations, all involving the $h_{11/2}$ proton, are expected to be lower in energy than the $g_{9/2}^{-1}h_{11/2}$ configuration. The $g_{9/2}^{-1}h_{11/2}$ configuration is predicted to have a quadrupole deformation of $\beta_2 = 0.26$ before the neutron $(h_{11/2})^2$ alignment. This deformation is about 10% larger than those for the lower negative-parity proton configurations. The band interaction and crossing frequency also depend on deformation. Since the surface is rather soft and it is difficult to trace the $g_{9/2}^{-1}h_{11/2}$ configuration over a larger frequency range, one cannot say which effects are dominant in the alignment behaviour of the different negative-parity side bands. The band interaction observed in the $\pi h_{11/2}$ and $\pi g_{9/2}h_{11/2}$ bands is, however, larger than those obtained from the CSM. The identical bands of ^{117,119}I and ^{118,120}Xe imply similar angular momentum increase, i.e. similar interaction with the aligned $(h_{11/2})^2$ neutrons. However, since the predicted equilibrium deformation is rather different for the 2qp and 1qp configurations, respectively, it is not possible to understand this behaviour within the present mean-field approach.

4.2.4. Decoupled negative-parity bands. The negative-parity bands 2 and 3 in ^{118}Xe are very similar, c.f. Figs. 8 and 9. The aligned angular momentum increases gradually up to $\hbar\omega = 0.41$ MeV. Above that frequency these bands show band crossings; band 2 at $\hbar\omega \approx 0.44$ MeV and band 3 at $\hbar\omega \approx 0.43$ MeV. The alignment gains are about $4\hbar$. Band 2 experiences another crossing around $I^\pi = 27^-$ at a rotational frequency of 0.58 MeV. Due to the similarities in the alignment curves for these bands, it is tempting to interpret them as signature partners. The energy splitting between bands 2 and 3 is about 320 keV at $\hbar\omega = 0.30$ MeV, whereas at $\hbar\omega = 0.50$ MeV it has decreased to 200 keV.

The low-spin part of bands 2 and 3 in ^{120}Xe resembles very much the corresponding bands in ^{118}Xe, indicating similar internal structure. In the crossing region, however, the corresponding bands of the two nuclei behave differently. While relatively sharp crossings are observed in ^{118}Xe, only very gradual gains in the aligned angular momenta take place in ^{120}Xe. The slope of the alignment curve is largest at about $\hbar\omega = 0.49$ MeV in both bands in ^{120}Xe, indicating similar crossing frequencies. The observation of the $\Delta I = 1$ transitions from band 3 to band 2 in ^{120}Xe also suggests that these bands are signature partners.

It is very difficult to distinguish between the proton and neutron excitations in the Xe-region, since in both cases one expects the $h_{11/2}$ alignment at similar frequencies and thus one cannot use blocking arguments. The very soft energy surface puts additional difficulties to the interpretation of the negative-parity structures. In the following, an attempt is made to explain the nature of the lowest excitations and to obtain a consistent picture.

Low-lying bands built on orbitals emanating from $g_{7/2}h_{11/2}$ and $d_{5/2}h_{11/2}$ are expected in the $A \approx 120$ Xe-nuclei for both neutrons and protons. Furthermore, a band built on the neutron $d_{3/2}h_{11/2}$ configuration might be found at low excitation energy in the even Xe-nuclei with $A \geqslant 120$. The fact that the $\alpha = 1$ band (band 2) is lower in energy than the $\alpha = 0$ band (band 3) suggests the $g_{7/2}h_{11/2}$ (or $d_{3/2}h_{11/2}$) configuration. Since in ^{117}I and ^{119}I one observes the $d_{5/2}$ and $g_{7/2}$ quasiproton states at lower energy than the $g_{9/2}$ state [43], we would expect the analogous band heads of the proton $g_{7/2}h_{11/2}$ and $d_{5/2}h_{11/2}$ bands to be found at lower energies than the band head of the proton $g_{9/2}^{-1}h_{11/2}$ band. At low spin the lowest negative-parity bands in the neighbouring Ba-nuclei [6,28,39] have properties very similar to those of bands 2 and 3. Based on blocking arguments these bands have been interpreted to have a proton character. It is most likely that also in ^{118}Xe and ^{120}Xe the observed decoupled negative-parity bands are built on the proton $g_{7/2}h_{11/2}$ configuration. This is supported by the routhians, by the branching ratios and by the configuration mixing analysis of bands 1 and 2 in ^{120}Xe, as discussed later.

The TRS calculations predict that the lowest negative-parity proton 2qp configuration lies about 300 keV lower in energy than the corresponding neutron configuration. In the TR surfaces the $\alpha = 1$ signature is clearly favoured for the protons, whereas for the neutrons the ordering of the EA and EB configurations sensitively depends on the neutron number and the deformations. For the low-K proton $\frac{3}{2}^+[422]$ configuration the CSM calculation give (at $\hbar\omega = 0.30$ MeV) a signature splitting of about 300 keV in agreement with the experimental splitting between bands 2 and 3 (see Fig. 9). For the lowest 2qp neutron configurations the standard CSM calculations indicate signature splittings up to about 200 keV (at $\hbar\omega = 0.30$ MeV). The signature splitting of bands 2 and 3 thus favour the proton scenario. The calculations predict that the optimum quadrupole deformation is 0.22–0.23 for both the lowest proton and neutron 2qp negative-parity configurations. These configurations favour quite different triaxial shapes; clearly positive γ for the protons and negative γ for the neutrons, c.f. Table 4. On the neutron side the assignment is very complicated, since in the theoretical routhians calculated at appropriate deformation the $\frac{5}{2}^+[402]$, $\frac{5}{2}^+[413]$ and $\frac{1}{2}^+[411]$ orbitals lie within 100 keV. In the case of the proton assignment, the close lying $\frac{1}{2}^+[420]$ and $\frac{3}{2}^+[431]$ states are pseudo-spin partner orbitals, which will mix accordingly. This is the case especially for the $\alpha = 0$ branch, which will be a mixture of the favoured sequence of the $\frac{1}{2}^+[420]$ and the unfavoured sequence of the $\frac{3}{2}^+[431]$ configurations.

The discussed proton and neutron $g_{7/2}h_{11/2}$ ($d_{5/2}h_{11/2}$) bands are predicted to have larger aligned angular momentum than the proton $g_{9/2}^{-1}h_{11/2}$ band. Below $\hbar\omega \approx 0.40$ MeV bands 2 and 3 in ^{118}Xe and ^{120}Xe are, however, associated with a smaller aligned angu-

lar momentum than the proton $g_{9/2}^{-1}h_{11/2}$ band. One should note that the $\frac{1}{2}^+[420]$ and $\frac{1}{2}^-[550]$ configurations can become mixed by the coupling to the octupole vibrational band. The rather low excitation energy as well as the initial alignment being around $3\hbar$, suggest that the low-spin states of bands 2 and 3 may be described in terms of an octupole vibrational character, which in the course of rotation changes into two-quasiparticle-like proton excitation. This scenario is very analogous to the one described by Neergård and Vogel [44,45], see also similar bands in ^{164}Yb [46] and in the Os–W region [47]. The role of the octupole correlations in the neighbouring even Ba-nuclei has been discussed in refs. [48,49].

The presence of the octupole correlations is indicated by enhanced E1 transitions between the negative-parity bands 2 and 3, and the ground-state band. Using a quadrupole moment of $Q_t = 3.7\ e\cdot$b and the experimental branching ratios, reduced transition probabilities of $B(E1) \approx 2\text{–}3 \times 10^{-4} e^2\text{fm}^2$ are obtained for bands 2 and 3 in ^{118}Xe and ^{120}Xe. Structures suggestive of octupole deformation have been observed in ^{144}Ba [50]. The $B(E1)$ transition rates deduced for ^{118}Xe and ^{120}Xe are about 10% of those in ^{144}Ba, but still very large. Calculations for the heavier even Xe-nuclei and the neighbouring Ba-nuclei give similar results. These finding suggest that octupole correlations play a role in the decoupled sequences in the Xe–Ba region. However, this needs to be confirmed by lifetime measurements.

The very smooth alignment process observed in ^{120}Xe, which is very similar to the one observed in the $h_{11/2}$ proton bands in ^{121}Cs [5], further supports the proton $g_{7/2}h_{11/2}$ assignment. Whether the difference in the band-crossing region between ^{120}Xe and ^{118}Xe originate from a different interaction strength with the aligned neutron configuration or with the octupole vibrational band, is beyond the scope of the present investigation.

The calculated neutron $(h_{11/2})^2$ alignment in the proton $g_{7/2}h_{11/2}$ bands takes place at $\hbar\omega \approx 0.35$ MeV both in ^{118}Xe and ^{120}Xe, which is rather far from the experimental values. This shows the problem of the neutron-crossing frequencies, which are too low in the CSM calculations. In conclusions, the TRS calculations are able to follow general trends, created by the change in shape and associated changes in the single-particle content. However, they fail to reproduce fine details of the experimental data, especially the neutron crossing frequency.

4.2.5. Terminating states. The yrast sequence in ^{118}Xe shows a sharp upbend around spins $I = 26\text{–}32$, which was interpreted in terms of a band termination. Similar states were also observed in ^{122}Xe [30] and ^{121}I [51]. TRS calculations indeed predict low lying 32^+ and 36^+ states associated with the $\pi(h_{11/2})^2(g_{7/2})^2_{16+} \otimes \nu(h_{11/2})^4(g_{7/2})^2_{16+,20+}$ configurations. Since the neutron states involve many 2p2h excitations, one does not expect the terminating states to be as favoured as in ^{122}Xe, where the neutrons occupy only four $h_{11/2}$ states outside the $N = 64$ core. In ^{118}Xe, the terminating states will cross the collective states first at spin 36 according to the TRS calculations. However, a structure with reduced collectivity and positive γ-values ($\gamma = 10°\text{–}16°$) crosses the yrast structure around spin $I = 28$. The reduced collectivity results in a larger effective

angular momentum alignment and the observed crossing might thus be associated with a change in shape towards positive γ and smaller β_2. At a triaxial (or oblate) shape the $g_{9/2}$ orbital is below the Fermi surface and stays essentially occupied, implying that only four protons are excited outside the $Z = 50$ core, hence yielding a smaller quadrupole deformation. Whether this structure will connect to the favoured non-collective 36^+ state is beyond the present experimental investigation. Note that the $g_{9/2}$ hole states strongly favour prolate shapes, in contrast to the terminating or triaxial structures, where the $g_{9/2}$ subshell essentially is occupied and where the favoured signature of the proton $h_{11/2}$ orbital drives the nucleus towards positive γ and oblate shapes.

Similarly, in the negative-parity states, one observes rather sharp crossings in the $\alpha = 1$ structure at $\hbar\omega = 0.58$ MeV. Again, from the TRS calculations, one finds favoured terminating states at $I = 25$, 27 and 29 involving the $\pi(g_{7/2}h_{11/2})_{9^-}$ state coupled to the $I = 16$, 18 and 20 neutron states of the $(h_{11/2})^2(g_{7/2})^2(d_{5/2})^2$ origin. These states are connected through a very soft surface to the collective rotational bands, and it is possible that at $\hbar\omega = 0.58$ MeV we are actually entering the non-collective regime. An alternative explanation for this upbend in band 2 would involve the first non-blocked $h_{11/2}$ proton crossing.

4.2.6. Configuration mixing between bands 1 and 2 in ^{120}Xe. Odd-spin states of band 1 in ^{120}Xe lie very close in excitation energy to the states in band 2 with the same spin values. Near the bottom of the bands and above $I = 17$ the states in band 2 are lower, whereas for the 13^-, 15^- and 17^- states the ordering is reversed. In this region the observed interband transitions indicate configuration mixing. The energy difference for the 13^- states is 13 keV, which gives an upper limit of 6.5 keV for the interaction strength. The 11^- states are 57 keV apart and assumed to be unmixed. At spin 17 the two states are only 10 keV apart. However, no interband transitions are observed, probably because of intensity limitations in the present experiment. We performed a two-level model mixing analysis, following the prescription of ref. [52], where the interaction strength between the proton $h_{9/2}$ and $h_{11/2}$ configurations in ^{163}Tm was determined to be about 7 keV. Our analysis for ^{120}Xe yields an interaction of ≈ 4 keV, which agrees with the values obtained from the CSM for the proton configuration. In the CSM calculations the difference in shape of the different configurations is neglected, and therefore a comparison of calculated values with experiment is associated with uncertainties. On the other hand, if the negative-parity side bands are all of neutron origin, the interaction strength is expected to be larger, since the relevant neutron orbitals differ less in their K-values. If, however, band 2 is of neutron origin, and the strongly coupled band of proton origin, the interaction cannot be determined from the CSM, since it now relates to the neutron–proton interaction, which is beyond our present model.

4.3. NUCLEUS ^{117}Xe

The ground state of ^{117}Xe has been assigned to have spin and parity $\frac{5}{2}^+$. Following the discussion in subsect. 3.1 we associate the ground state and in consequence band 3

with the $\frac{5}{2}^+[402]$ Nilsson label. At the calculated equilibrium deformation of $\beta_2 \approx 0.24$, the pseudo-spin partner orbitals $\frac{3}{2}^+[411]$, $\frac{5}{2}^+[413]$ are very close to the Fermi surface, while the $\frac{5}{2}^+[402]$ and $\frac{1}{2}^+[411]$ orbitals are slightly further away. The $\frac{5}{2}^+[413]$ and $\frac{1}{2}^+[411]$ configuration favour the $\alpha = -\frac{1}{2}$ sequence, but only the latter configuration is associated with sizable signature splitting. Since the signature splitting in band 4 is very small, we associate this structure with the $\frac{5}{2}^+[413]$ configuration.

According to the TRS calculations the two lowest signatures of the positive-parity orbitals posses similar shapes and is calculated to stretch in a similar way as the yrast sequence in ^{118}Xe. However, the surface is very soft in the β_2-direction. The neutron $h_{11/2}$ alignment is calculated to be lowest in frequency, and will drive the nucleus to negative γ-values and smaller β_2.

In band 4, the alignment gain of about $3\hbar$ at 0.33 MeV is too small for either the proton or the neutron $h_{11/2}$ alignment. However, the total alignment gain between $\hbar\omega = 0.1$ MeV and $\hbar\omega = 0.4$ MeV might very well reflect such a band crossing. The smooth increase in angular momenta below $\hbar\omega = 0.3$ MeV might then correspond to a stretching and possible smooth onset of the $h_{11/2}$ neutron alignment, which then drives the nucleus towards negative γ-values. Note that such a shape change also induces a signature splitting which thus might explain why the unfavoured signature is not observed to higher spins.

The two $\frac{7}{2}^+$ states are only 8.1 keV apart. A similar analysis as in the previous subsection gives an interaction strength of 3.7 keV for these states. This indicates that bands 4 and 3 have more differences than just their single-particle content. An inspection of a relevant Nilsson diagram yields that the $\frac{5}{2}^+[402]$ state is close to the Fermi surface at rather small $\beta_2 \approx 0.15$, and in consequence one can expect different shapes for the two positive-parity band structures.

The negative-parity band 1 is associated with either the $\frac{5}{2}^-[532]$ or $\frac{3}{2}^-[541]$ configuration. This band has a large initial alignment (c.f. Fig. 8) as expected for the $h_{11/2}$ neutrons. The favoured $\alpha = -\frac{1}{2}$ band is crossed by a 3qp band at $\hbar\omega = 0.45$ MeV. The alignment gain is about 5–$6\hbar$. In the unfavoured $\alpha = \frac{1}{2}$ branch the band-crossing frequency cannot be extracted. The slight increase in the alignment at the last observed transition suggests that the band crossing might occur at a lower frequency than in the favoured band. The alignment of the lowest $h_{11/2}$ neutron pair (EF) is blocked in band 1. Thus the observed band crossing is caused by the alignment of the $h_{11/2}$ protons (ef) or by the alignment of the first non-blocked $h_{11/2}$ neutron pair (FG). The observed crossing frequency in band 1 is larger than those found for the $h_{11/2}$ bands in ^{121}Ba, where the favoured and unfavoured signatures have backbends at $\hbar\omega = 0.38$ MeV and $\hbar\omega = 0.35$ MeV, respectively. These band crossings have been attributed to the $h_{11/2}$ protons [7].

The energy splitting between the favoured and unfavoured signatures of the $h_{11/2}$ band in ^{117}Xe is predicted by the TRS calculations to be 320 keV at $\hbar\omega = 0.30$ MeV, which is close to the experimental signature splitting of 380 keV. The unfavoured signature has a slightly larger β_2 and a less negative γ-value than the favoured signature partner. The shape for the unfavoured signature partner is, in fact, similar to that of the g.s. bands in ^{118}Xe and ^{120}Xe. The effect of such a shape difference for the band-crossing behaviour

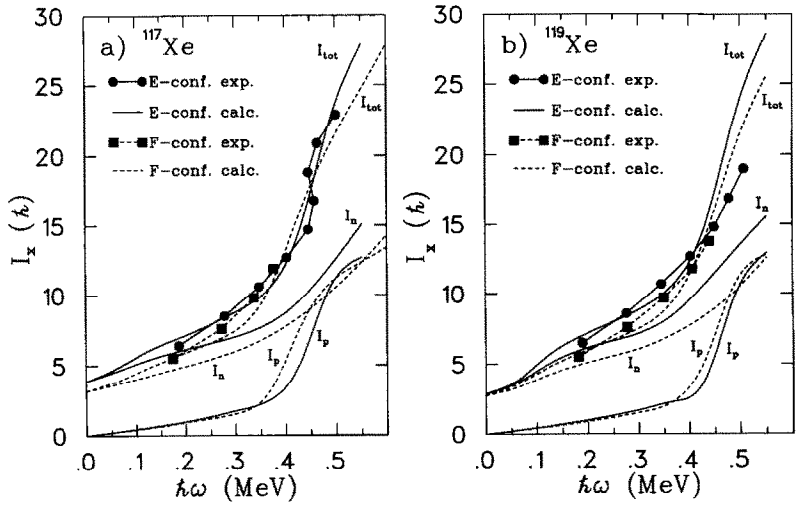

Fig. 14. Experimental and calculated I_x versus $\hbar\omega$ for both signatures of the $\frac{5}{2}^-[532]$ band. (a) ^{117}Xe; (b) ^{119}Xe.

is demonstrated in Fig. 14a, showing I_x for the favoured and unfavoured signatures of the $h_{11/2}$ band as a function of rotational frequency. The experimental quantity I_x is calculated as $I_x = \sqrt{I(I+1) - K^2}$. The theoretical I_x curves show upbends at the rotational frequencies of 0.40–0.50 MeV. The protons, as well as the neutrons contribute to these alignment gains. The proton ef alignment is relatively sharp and gives about $7\hbar$ units of aligned angular momentum. It takes place at $\hbar\omega = 0.45$ MeV in the E-configuration, whereas it occurs somewhat earlier in the F-configuration, 0.42 MeV. The neutron FG alignment ($\hbar\omega \approx 0.5$ MeV) in the favoured signature, as well as the EH alignment ($\hbar\omega \approx 0.5$ MeV) in the unfavoured signature, is gradual and gives little angular momentum. Therefore, we associate the observed strong band crossing mainly with the alignment of the $(h_{11/2})^2$ protons.

For comparison the experimental and theoretical spin I_x for the neutron $h_{11/2}$ band in ^{119}Xe [53] are shown in Fig. 14b. Instead of the strong band crossing observed in ^{117}Xe in the favoured $\alpha = -\frac{1}{2}$ signature, the experimental I_x curve for ^{119}Xe shows only a slight increase around $\hbar\omega \approx 0.50$ MeV. This change in the band-crossing behaviour is at least partly explained by the TRS calculations. The calculations predict that the optimum γ-deformation becomes more negative with increasing N. Therefore the FG alignment comes somewhat earlier and the proton ef alignment later in ^{119}Xe than in ^{117}Xe.

4.4. ANALYSIS OF BRANCHING RATIOS

The $\Delta I = 2/\Delta I = 1$ branching ratios within rotational bands can yield valuable information about the quasiparticle configuration of the band. Experimental values for the ratio of reduced magnetic dipole and stretched electric quadrupole transition probabilities

TABLE 5
Summary of parameters used in calculating the $B(M1)/B(E2)$ ratios

Configuration	g-factor	K	$i_x(\hbar)$
$\nu d_{5/2}$	−0.33	2.5	0.5
$\nu g_{7/2}$	0.21	2.5	1.0
$\nu d_{3/2}$	0.44	0.5	1.0
$\nu h_{11/2}$	−0.21	2.5	4.0
$\pi g_{7/2}$	0.72	1.5	1.0
$\pi g_{9/2}$	1.27	4.5	0.0
$\pi h_{11/2}$	1.17	0.5	5.0

can be extracted by using the expression

$$\frac{B(M1;I \to I-1)}{B(E2;I \to I-2)} = 0.697 \frac{(E_\gamma(I \to I-2))^5}{(E_\gamma(I \to I-1))^3 \lambda}, \tag{2}$$

where λ is the intensity ratio for the stretched quadrupole and dipole transitions. The multipolarity mixing ratio δ of the $\Delta I = 1$ transitions has been neglected in this expression. The effect of δ is usually insignificant for the $B(M1)/B(E2)$ ratios.

Theoretical estimates for the $B(M1)/B(E2)$ ratios are obtained from the semiclassical formula [54,55]:

$$\begin{aligned}\frac{B(M1;I \to I-1)}{B(E2;I \to I-2)} = {} & \frac{12}{5Q_0^2 \cos^2(\gamma + 30) I^2} \left[1 - \frac{K^2}{(I - \frac{1}{2})^2}\right]^{-2} \\ & \times \Big\{ (I^2 - K^2)^{1/2} \Big[K_1 (g_1 - g_R)\left(1 \pm \Delta e'/\hbar\omega\right) \\ & + K_2 (g_2 - g_R) + K_3 (g_3 - g_R)\Big] \\ & - K\Big[(g_1 - g_R) i_1 + (g_2 - g_R) i_2 + (g_3 - g_R) i_3\Big]\Big\}^2 . \end{aligned} \tag{3}$$

The subscript 1 refers to the quasiparticle configuration which is responsible for the signature splitting. Subscripts 2 and 3 refer to the additional quasiparticles or to the pair of aligned quasiparticles. The K-value is taken as $K = K_1 + K_2 + K_3$. The parameters used in the calculations are listed in Table 5. For the rotational gyromagnetic factor g_R a value of 0.45 ($\approx Z/A$) was used, and the orbital gyromagnetic factors were taken from the compilation of Lönnroth et al. [56]. The value of the quadrupole moment (3.7 e·b) was derived from the deformations predicted by the TRS calculations (subsect. 4.1).

Experimental $B(M1)/B(E2)$ ratios for ^{117}Xe together with their theoretical estimates are displayed in Fig. 15a. In ^{117}Xe the branching ratios could only be obtained for the neutron $h_{11/2}$ band (band 1 in Fig. 1). The theoretical estimate reproduces the experimental data points better for $K = \frac{3}{2}$ than for $K = \frac{5}{2}$, but since the $\alpha_f \to \alpha_i$ transitions are lacking, it is difficult to determine the K-value. The CSM calculations at appropriate

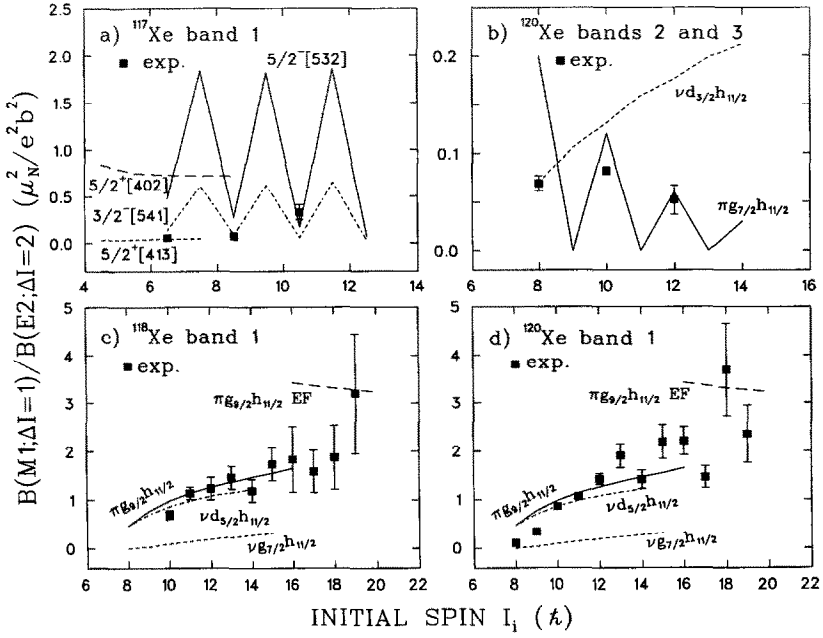

Fig. 15. Experimental and theoretical $B(\mathrm{M1};I \to I-1)/B(\mathrm{E2};I \to I-2)$ ratios in ^{117}Xe, ^{118}Xe and ^{120}Xe.

deformations and $\hbar\omega = 0.0$ MeV predict that the $\frac{5}{2}^-[532]$ orbital should be slightly closer to the Fermi surface than the $\frac{3}{2}^-[541]$ orbital. With increasing rotation the wave functions are expected to become more and more mixed, which results in a lowering of the effective K-value for the lowest $h_{11/2}$ band. For the positive-parity $\frac{5}{2}^+[402]$ band the theoretical estimate of the $B(\mathrm{M1})/B(\mathrm{E2})$ ratio is much larger than for the $\frac{5}{2}^+[413]$ band, supporting the configuration assignments made earlier.

We have extracted the $B(\mathrm{M1})/B(\mathrm{E2})$ ratios for band 1 in ^{118}Xe and ^{120}Xe and for bands 2/3 in ^{120}Xe. The theoretical estimates were calculated (with appropriate signature splittings) for the proton and neutron 2qp configurations involving the $h_{11/2}$ orbital coupled to one of the low-lying positive-parity orbitals. The positive-parity configuration was assumed to contribute to both signatures of the two-quasiparticle band.

The large $B(\mathrm{M1})/B(\mathrm{E2})$ ratios measured for band 1 in ^{118}Xe and ^{120}Xe are reproduced equally well by the proton $g_{9/2}^{-1}h_{11/2}$ and neutron $d_{5/2}h_{11/2}$ configurations, c.f. figs. 15c and 15d. The neutron $g_{7/2}h_{11/2}$ configuration, which is also associated with a small signature splitting, gives clearly too small $B(\mathrm{M1})/B(\mathrm{E2})$ ratios compared to the experimental values. At the highest spin values the experimental values start to exceed the theoretical predictions, which could be indicative of an alignment. For bands 2/3 in ^{120}Xe the experimental $B(\mathrm{M1})/B(\mathrm{E2})$ ratios are approximately reproduced by the proton $g_{7/2}h_{11/2}$ and the neutron $d_{3/2}h_{11/2}$ configurations.

The sign of the multipolarity mixing ratio for the $\Delta I = 1$ intraband transitions depends on the term inside the curly brackets in Eq. (2). In the 1qp bands this sign is given by the well-known relation, $\mathrm{sign}(\delta) = \mathrm{sign}((g_1 - g_R)/Q_0)$, which gives a negative sign for neutrons and a positive sign for protons, assuming a prolate shape. For the 2qp bands this holds only if the term inside the curly brackets is dominated by the DAL-term. In the case of band 1 in ^{118}Xe and ^{120}Xe, this is true both for the proton $g_{9/2}^{-1}h_{11/2}$ and $d_{5/2}h_{11/2}$ configurations. The DCO ratios measured for the $\Delta = 1$ transitions indicate positive sign of δ, which is thus consistent with the proton configuration. In the case of bands 2/3 in ^{120}Xe and the proton $g_{7/2}h_{11/2}$ configuration, the RAL-term is dominating and therefore we obtain $\delta < 0$. In the neutron $d_{3/2}h_{11/2}$ configuration the positive-parity orbital does not contribute to the sign of multipolarity mixing ratio ($g_1 - g_R \approx 0$) and $\delta < 0$ is obtained. Thus both of these configurations yield negative sign of the multipolarity mixing ratio, in agreement with the DCO ratios of the 507.7 and 564.4 keV transitions indicating $\delta \approx -0.4$.

The $B(E2; I \rightarrow I-1)/B(E2; I \rightarrow I-2)$ ratios within a band are very sensitive to the K-value. For bands 2/3 the measured $B(E2; I \rightarrow I-1)/B(E2; I \rightarrow I-2)$ ratios are consistent with $K = 1$–2, which also favours the proton $g_{7/2}h_{11/2}$ configuration.

5. Conclusions

Rotational bands of ^{117}Xe, ^{118}Xe and ^{120}Xe have been studied with the NORDBALL detector array. Together, about 15 bands were established and in many of them band crossings were observed. By comparing the band properties with known bands in the neighbouring nuclei, conclusions of the band configurations have been made. The analysis of the $\Delta I = 1/\Delta I = 2$ branching ratios within bands has contributed to the configuration assignments.

The yrast bands of ^{118}Xe and ^{120}Xe experience band crossings with very large gain in the alignment at $\hbar\omega = 0.39$ MeV. These crossings are interpreted as being caused by the simultaneous proton and neutron $(h_{11/2})^2$ alignments. An involvement of the proton alignment in the band crossing of the yrast bands, is also supported by the fact that a band crossing at a comparable frequency is observed in the neutron $h_{11/2}$ band in ^{117}Xe. The second positive-parity band (band 4), extended to high spins, has similar properties as the neutron S-bands observed in heavier even Xe-nuclei. The third positive-parity band in ^{120}Xe is a candidate for the γS-band.

Strongly coupled negative-parity bands have been observed in ^{118}Xe and ^{120}Xe. These structures could be associated with the proton $g_{9/2}^{-1}h_{11/2}$ configuration. The TRS calculations predict that the quadrupole deformation in this configuration is $\beta_2 = 0.26$, being 10% larger than in the other negative-parity bands. The behaviour of the decoupled negative-parity bands turned out to be difficult to interpret. We suggest that these bands have an octupole character at low spins which in the course of rotation gives way for the proton 2qp character. While the routhians, $B(M1; I \rightarrow I-1)/B(E2; I \rightarrow I-2)$ ratios and $B(E2; I \rightarrow I-1)/B(E2; I \rightarrow I-2)$ ratios are consistent with the proton

assignment, the observed band-crossing frequency is calculated to come too early in the TRS approach. This is analogous to the $i_{13/2}$ neutron crossing in the rare-earth region.

When comparing the ^{118}Xe and ^{120}Xe nuclei to the heavier Xe-isotopes, we observe sudden changes in the alignment patterns of the yrast bands, as well as in the character of the strongly coupled bands. These changes are related to the energy position of the particle–hole $\pi(g_{9/2})^{-2} \rightarrow \pi(h_{11/2})^2$ excitation, yielding well-deformed rotational structures. With increasing N the neutrons tend to polarize the nucleus towards a more oblate shape, and the excitations of the protons into the $h_{11/2}$ orbital become unfavourable. We observe identical bands in the strongly coupled two-quasiparticle proton configuration and the $h_{11/2}$ band in the odd-I isotones. This feature can certainly not be explained by our mean-field calculations.

This work was partially supported by the Academy of Finland, The Danish and Swedish Natural Science Research Councils and the NORDBALL collaboration. We are grateful to the staff of the Niels Bohr Institute, in particular Mrs. S. Dahl, Dr. G. Sletten, Mrs. J. Sørensen and Mr. J. Westergaard. We would also like to thank Drs. S.E. Arnell, H.A. Roth and Ö. Skeppstedt for the support with the liquid-scintillator detector wall. Software written by D.C. Radford was used in the data analysis.

References

[1] R. Wyss, A. Granderath, R. Bengtsson, P. von Brentano, A. Dewald, A. Gelberg, A. Gizon, J. Gizon, S. Harrissopulos, A. Johnson, W. Lieberz, W. Nazarewicz, J. Nyberg and K. Schiffer, Nucl. Phys. A 505 (1989) 337.
[2] G. Puddu, O. Scholten and T. Otsuka, Nucl. Phys. A 348 (1980) 109.
[3] T. Otsuka, Hyperfine Int.75 (1992) 23.
[4] S.T. Hsieh, H.C. Chiang, M.M. King Yen, Phys. Rev C 41 (1990) 2898.
[5] F. Lidén, B. Cederwall, P. Ahonen, D.W. Banes, B. Fant, J. Gascon, L. Hildingsson, A. Johnson, S. Juutinen, A. Kirwan, D.J.G. Love, S. Mitarai, J. Mukai, A.H. Nelson, J. Nyberg, J. Simpson and R. Wyss, Nucl. Phys. A 550 (1992) 365.
[6] B. Cederwall, A. Johnson, R. Wyss, F. Lidén, B. Fant, S. Juutinen, P. Ahonen, S. Mitarai, J. Mukai and J. Nyberg, Z. Phys. A 338 (1991) 461.
[7] B. Cederwall, A. Johnson, R. Wyss, C.G. Lindén, S. Mitarai, J. Mukai, B. Fant, S. Juutinen, P. Ahonen and J. Nyberg, Nucl. Phys. A 529 (1991) 410.
[8] B. Cederwall, A. Johnson, B. Fant, S. Juutinen, P. Ahonen S. Mitarai, J. Mukai and J. Nyberg, Z. Phys. A 338 (1991) 463.
[9] R. Wyss, F. Lidén, J. Nyberg, A. Johnson, D.J.G. Love, A.H. Nelson, D.W. Banes, J. Simpson, A. Kirwan and R. Bengtsson, Nucl. Phys. A 503 (1989) 244.
[10] C.B. Moon, J.C. Kim, J.U. Kwon, B.N. Sung, K. Furono, T. Komatsubara, T. Hosoda, T. Kaneko, S.C. Jeong, I. Kurniawan and T. Aoki, Nucl. Phys. A 510 (1990) 173.
[11] M.S. Rouabah, Th. Byrski, F.A. Beck, D. Curien, B. Haas, J.C. Merdinger, J.P. Vivien, J. Gizon and B. Nyakó, Z. Phys. A 328 (1987) 493.
[12] P. Chowdhury, U. Garg, T.P. Sjoreen and D.B. Fossan, Phys. Rev. C 23 (1981) 733.
[13] G. Marguier, C. Richard-Serre, J. Genevey, M. Morgue, A. Charvet, J. Giroux, A. Huck, A. Knipper and G. Walter, J. of Phys. G12 (1986) 757.
[14] K. Loewenich, K.O. Zell, A. Dewald, W. Gast, A. Gelberg, W. Lieberz, P. von Brentano and P. van Isacker, Nucl. Phys. A 460 (1986) 361.

[15] J. Goswamy, A. Sharma, D. Mehta, B. Chand, N. Singh, P.N. Trehan, P. Singh, R.G. Pilley, H.G. Devare, R.K. Bhowmik and C.R. Praharaj, Z. Phys. A 344 (1992) 233.
[16] S. Juutinen, S. Törmänen, B. Cederwall, A. Johnson, R. Julin, S. Mitarai, J. Mukai, P. Ahonen, B. Fant, F. Lidén, J. Nyberg and I. Ragnarsson, Z. Phys. A 338 (1991) 365.
[17] S. Juutinen, S. Törmänen, P. Ahonen, B. Cederwall, B. Fant, A. Johnson, R. Julin, S. Mitarai, J. Mukai, J. Nyberg, M. Piiparinen, A. Virtanen and R. Wyss, Nucl. Phys. A 553 (1993) 531.
[18] T. Kuroyanagi, S. Mitarai, K. Suematsu, B.J. Min, H. Tomura, J. Mukai, T. Maeda, R. Nakatani, G. Sletten, J. Nyberg and D. Jerrestam, Nucl. Instr. Meth. A 316 (1992) 289.
[19] S.E. Arnell, H.A. Roth, Ö. Skeppstedt, J. Bialkowski, M. Moszyński, D. Wolski and J. Nyberg, Nucl. Instr. Meth. A 300 (1991) 303.
[20] B. Cederwall, F. Liden, A. Johnson, L. Hildingsson, R. Wyss, B. Fant, S. Juutinen, P. Ahonen, S. Mitarai, J. Mukai, J. Nyberg, I. Ragnarsson, P.B. Semmes, Nucl. Phys. A 542 (1992) 454.
[21] J. Blachot and G. Marguier, Nucl. Data Sheets 66 (1992) 451.
[22] V. Barci, J. Gizon, A. Gizon, J. Crawford, J. Genevey, A. Plochocki and M.A. Cunningham, Nucl. Phys. A 383 (1982) 309.
[23] R. Bengtsson and S. Frauendorf, Nucl. Phys. A 314 (1979) 27; A 327 (1979) 139.
[24] R.A. Wyss, A. Johnson, J. Nyberg, R. Bengtsson and W. Nazarewicz, Z. Phys A 329 (1988) 255.
[25] S. Juutinen, S. Törmänen, P. Ahonen, B. Cederwall, A. Johnson, B. Fant, R. Julin, S. Mitarai, J. Mukai, J. Nyberg and A. Virtanen, Z. Phys. A 344 (1992) 223.
[26] R. Wyss and A. Johnson, Proc. Int. Conf. on high spin physics and gamma-soft nuclei, Pittsburg 1990 (World Scientific, Singapore, 1991) p. 123.
[27] E.S. Paul, M.P. Waring, R.M. Clark, S.A. Forbes, D.B. Fossan, J.R. Hughes, D.R. LaFosse, Y. Liang, R. Ma, P. Vaska and R. Wardworth, Phys. Rev. C 45 (1992) 2531.
[28] R. Wyss, A. Johnson, F. Liden, J. Nyberg, A.H. Nelson, D.W. Banes, A. Kirwan, D.J.G. Love and J. Simpson, Proc. XXV Int. Winter Meeting on nuclear physics, Bormio, January 1987, ed. I. Iori, p. 542.
[29] J. Hattula, S. Juutinen, M. Jääskeläinen, T. Lönnroth, A. Pakkanen, M. Piiparinen and G. Sletten, J. of Phys. G13 (1987) 57.
[30] J. Simpson, H. Timmers, M.A. Riley, T. Bengtsson, M.A. Bentley, F. Hanna, S.M. Mullins, J.F. Scharpey-Schafer and R. Wyss, Phys. Lett. B 262 (1991) 388.
[31] W. Gast, U. Kaup, H. Hanewinkel, R. Reinhardt, K. Schiffer, K.P. Schmittgen, K.O. Zell, J. Wrzesinski, A. Gelberg and P. von Brentano, Z. Phys. A 318 (1984) 123.
[32] W. Lieberz, S. Freund, A. Granderath, A. Gelberg, A. Dewald, R. Reinhardt, R. Wirowski, K.O. Zell and P. von Brentano, Z. Phys. A 330 (1988) 221.
[33] M. Diebel, Nucl. Phys. A 419 (1984) 221.
[34] Y.R. Shimizu and K. Matsuyanagi, Prog. Theor. Phys. 70 (1983) 144; 72 (1984) 799.
[35] M. Matsuzaki, Nucl. Phys. A 509 (1990) 269.
[36] D. Ward, V.P. Janzen, H.R. Andrews, D.C. Radford, G.C. Ball, D. Horn, J.C. Waddington, J.K. Johansson, F. Banville, J. Gascon, S. Monaro, N. Nadon, S. Pilotte, D. Prevost, P. Taras and R. Wyss, Nucl. Phys. A 529 (1991) 315.
[37] H.R. Andrews, D. Ward, R.L. Graham and J.S. Geiger, Nucl. Phys. A 219 (1974) 141.
[38] R.F. Casten and P. von Brentano, Phys. Lett. B 152 (1985) 22.
[39] J.P. Martin, V. Barci, H. El-Samman, A. Gizon, J. Gizon, W. Klamra, B.M. Nyakó, F.A. Beck, Th. Byrski and J.C. Merdinger, Nucl. Phys. A 489 (1988) 169.
[40] Y. Liang, D.B. Fossan, J.R. Hughes, D.R. LaFosse, T. Lauritsen, R. Ma, E.S. Paul, P. Vaska, M.P. Waring and N. Xu, Phys. Rev. C 45 (1992) 1041.
[41] R. Wyss and W. Satula, Lund preprint Lund-MPh-93/05, submitted to Phys. Lett. B.
[42] W. Satula, R. Wyss and F. Dönau, Nucl. Phys. A 565 (1993) 573.
[43] M. Gai, D.M. Gordon, R.E. Shroy, D.B. Fossan, A.K. Gaigalas, Phys. Rev. C 26 (1982) 1101.
[44] K. Neergård and P. Vogel, Nucl. Phys. A 145 (1970) 33; A 149 (1970) 217.
[45] P. Vogel, Phys. Lett. B 60 (1976) 431.

[46] S. Jónsson, N. Roy, H. Ryde, W. Waluś, J. Kownacki, J.D. Garrett, G.B. Hagemann, B. Herskind, R. Bengtsson and S. Åberg, Nucl. Phys. A 449 (1986) 537.
[47] G.D. Dracoulis, Int. Conf. on nuclear behaviour at high angular momentum, Strasbourg, Suppl. J. de Phys. C 10 (1980) 66.
[48] R. Wyss, A. Johnson, D.J.G. Love, M.J. Godfrey and S.M. Mullins, Z. Phys. A 332 (1989) 241.
[49] K. Schiffer, A. Dewald, A. Gelberg, R. Reinhardt, K.O. Zell, Sun Xianfu and P. von Brentano, Z. Phys. A 327 (1987) 251.
[50] W.R. Phillips, I. Ahmad, H. Emling, R. Holzmann, R.V. Janssens and T.-L. Khoo, Phys. Rev. Lett. 57 (1986) 3257.
[51] Y. Liang, D.B. Fossan, J.R. Hughes, D.R. LaFosse, T. Lauritsen, R. Ma, E.S. Paul, P. Vaska, M.P. Waring, N. Xu and R.A. Wyss, Phys. Rev. C 44 (1991) 578.
[52] H.J. Jensen, G.B. Hagemann, P.O. Tjøm, S. Frauendorf, A. Atac, M. Bergström, A. Bracco, A. Brockstedt, H. Carlsson, P. Ekström, J.M. Espino, B. Herskind, F. Ingebretsen, J. Jongman, S. Leoni, R.M. Lieder, T. Lönnroth, A. Maj, B. Million, A. Nordlund, J. Nyberg, M. Piiparinen, H. Ryde, M. Sugavara and A. Virtanen, Z. Phys. A 340 (1992) 351.
[53] V.P. Janzen, M.P. Carpenter, L.L. Riedinger, W. Schmitz, D.G. Popescu, J.A. Cameron, J.K. Johansson, D.D. Rajnauth, J.C. Waddington, G. Kajrys, S. Monaro and S. Pilotte, Phys. Rev. C 39 (1989) 2050.
[54] F.Dönau and S. Frauendorf, in Proc. Conf. on high angular momentum properties of nuclei, Oak Ridge 1982, ed. N.R. Johnson (Harwood, New York, 1983) p. 143.
[55] D.C. Radford, H.R. Andrews, G.C. Ball, D. Horn, D. Ward, F. Banville, S. Flibotte, S. Monaro, S. Pilotte, P. Taras, J.K. Johansson, D. Tucker, J.C. Waddington, M.A. Riley, G.B. Hagemann and I. Hamamoto, Nucl. Phys. A 545 (1992) 665.
[56] T. Lönnroth, S. Vajda, O.C. Kistner and M.H. Rafailovich, Z. Phys. A 317 (1984) 215.